Delft University of Technology

The Actuator Disc Concept

van Kuik, G. A.M.

DOI
10.1007/978-3-030-31307-4_2

Publication date
2022

Document Version
Final published version

Published in
Handbook of Wind Energy Aerodynamics

Citation (APA)
van Kuik, G. A. M. (2022). The Actuator Disc Concept. In *Handbook of Wind Energy Aerodynamics: With 678 Figures and 33 Tables* (pp. 47-94). Springer. https://doi.org/10.1007/978-3-030-31307-4_2

Important note
To cite this publication, please use the final published version (if applicable).
Please check the document version above.

Copyright
Other than for strictly personal use, it is not permitted to download, forward or distribute the text or part of it, without the consent of the author(s) and/or copyright holder(s), unless the work is under an open content license such as Creative Commons.

Takedown policy
Please contact us and provide details if you believe this document breaches copyrights.
We will remove access to the work immediately and investigate your claim.

This work is downloaded from Delft University of Technology.
For technical reasons the number of authors shown on this cover page is limited to a maximum of 10.

Green Open Access added to TU Delft Institutional Repository

'You share, we take care!' - Taverne project

https://www.openaccess.nl/en/you-share-we-take-care

Otherwise as indicated in the copyright section: the publisher is the copyright holder of this work and the author uses the Dutch legislation to make this work public.

The Actuator Disc Concept

3

G. A. M. van Kuik

Contents

Introduction . . . 48
The Actuator Disc . . . 48
From Actuator Disc to Rotor Aerodynamics . . . 50
Force Fields in Rotor Aerodynamics . . . 51
Force Fields: Output from or Input in the Equation of Motion? . . . 51
Equivalence of the Kinematic and Dynamic Methods . . . 51
The Equation of Motion and the Coordinate Systems . . . 53
Non-conservative and Conservative Force Fields . . . 55
The Disc as Representation of a Rotor . . . 57
The Actuator Disc Equation . . . 57
Power and Thrust Expressions of Joukowsky Discs and Rotors . . . 59
Analysis of Froude Actuator Disc Flows . . . 64
The Momentum Balance . . . 65
Momentum Theory Without Conservative Forces . . . 66
Momentum Theory Including Conservative Forces . . . 67
Numerical Assessment of Actuator Disc Performance . . . 68
Flow and Pressure Patterns . . . 69
Properties of the Wake Boundary . . . 69
Pressure at the Axis . . . 71
The Velocity Distribution at the Disc . . . 72
The Momentum Balance Per Annulus . . . 74
An Engineering Model for the Velocity at the Disc . . . 75
Analysis of Joukowsky Actuator Disc Flows . . . 76
The Equations for a Disc with Torque and Swirl . . . 77
Momentum Theory for Joukowsky Discs . . . 80
Limit Values: $\lambda \to \infty$, $\lambda \to 0$, $C_{p,\max}$ . . . 82
Numerical Results . . . 84
The Momentum Balance Per Annulus of Joukowksy Disc Flows . . . 86

G. A. M. van Kuik (✉)
Faculty of Aerospace Engineering, Delft University of Technology, Delft, The Netherlands
e-mail: g.a.m.vankuik@tudelft.nl

© Springer Nature Switzerland AG 2022

B. Stoevesandt et al. (eds.), *Handbook of Wind Energy Aerodynamics*,
https://doi.org/10.1007/978-3-030-31307-4_2

The Role of Swirl . . . 88
On the Use of Actuator Disc Theory in BEM . . . 88
Blade and Tip Effects . . . 88
Comparison of Actuator Disc and BEM Induction . . . 89
Cross-References . . . 91
References . . . 91

Abstract

Actuator disc theory is the simplest rotor theory possible: the rotor is replaced by a permeable disc carrying an axisymmetric force field. It is more than a century old, with a first analytical result obtained by Froude in 1889. In 1918 Joukowsky published the first rotor performance prediction for a helicopter rotor in hover; in 1920 Betz and Joukowsky published the maximum efficiency of wind turbine rotors. In modern rotor design codes, this momentum theory still forms the basis, be it with many adaptations and engineering add-ons. This chapter treats the actuator disc theory in two versions. Best known is the classical theory relating to an actuator disc with thrust acting against the flow but without torque, so without wake swirl. This theory gives the Betz-Joukowsky limit. The results deviate when applied to a flow annulus instead of the entire stream tube, due to the role of the pressure exerted by one annulus to the other. The momentum theory for discs with thrust and torque is relevant for rotors operating with high torque at low rotational speed. For increasing rotational speed, the performance increases from zero to the Betz-Joukowsky limit. In all flow cases, with or without torque, the velocity vector in the meridional plane appears to be constant at the disc. For the performance per annulus and the performance with torque, the deviation from the classical momentum theory is explained by classifying force fields as conservative or non-conservative and investigating their impact on energy and momentum balances.

Keywords

Actuator disc · Momentum theory · Conservative forces · Non-conservative forces · Betz-Joukowsky · Induction · Velocity at the disc · Performance

Introduction

The Actuator Disc

Rotor aerodynamics has a history of more than a century, with the concept of the actuator disc to represent the action of a propeller formulated by Froude (1889). In this concept the disc carries only thrust, no torque. Based on this Joukowsky (1918) published the first performance prediction that still holds today, for a "static" rotor like a hovering helicopter rotor or propeller in still fluid. Two years later Joukowsky (1920) and Betz (1920) published the optimal performance of discs representing

wind turbines, for which reason it is called the Betz-Joukowsky maximum; see Okulov and van Kuik (2012). The names of these pioneers are also connected with the two concepts for actuator discs with thrust ánd torque. Betz (1919) proposed a vortex model for rotors equivalent to Prandtl's model of a wing with an elliptically distributed load, giving a uniform induced velocity with minimum induced drag. Each of the rotor blades is replaced by a lifting line releasing a free vortex sheet with constant velocity in axial direction. Joukowsky (1912) developed the vortex model of a propeller based on a rotating horseshoe vortex. In his vortex theory, each of the blades is replaced by a lifting line about which the circulation, associated with the bound vorticity, is constant.

The constant circulation model of Joukowsky and the constant velocity model of Betz were supposed to represent the ideal rotor. At the time of these pioneers, it was not yet possible to evaluate which model was more ideal than the other. Both models neglected wake expansion or contraction, so were valid only for lightly loaded rotors. Goldstein (1929) found an analytical solution for the wake of Betz's rotor restricted to lightly loaded propellers. Okulov et al. (2015, chapter 4) presented an overview of the development toward a complete non-linear solution to Betz's problem with wake expansion, including the non-linear solution of Okulov (2014). A similar solution was published by Wood (2015). Okulov et al. (2015, chapter 4) showed that Joukowsky rotors perform slightly better than Betz rotors for the same tip speed ratio. For the analyses in the next chapters, it is relevant to know that in the limit for an infinite number of blades rotating with infinite speed, both models converge to Froude's actuator disc and become identical.

Originally, the model of Betz-Goldstein is restricted to rotors with a finite number of blades, but it was extended to an infinite number of blades by Okulov (2014) and Wood (2015). It requires advanced vortex modelling, so the results are not easily used in state-of-the-art rotor design methods. An exception is the use of the Prandtl-Glauert tip correction which was derived by Prandtl based on Betz's model; see Glauert (1935, ch. VII-4) and section "Blade and Tip Effects." The constant circulation rotor model of Joukowsky is at the basis of many analysis and design methods used today; see, e.g., Burton et al. (2011, page 70) and van Kuik et al. (2015b). This model and the associated momentum theory will be evaluated in the present chapter.

The Joukowsky model has been studied in van Kuik (2018b) for discs representing wind turbine rotors as well as propellers, with emphasis on the fluid dynamic aspects. Here the emphasis is on the performance aspects of wind turbine actuator discs, preceded by the classification of the forces into conservative and non-conservative forces. This distinction is introduced as this appears to be helpful in the interpretation of the results. The main sections are sections "Analysis of Froude Actuator Disc Flows" and "Analysis of Joukowsky Actuator Disc Flows" where the performance of discs without torque, the Froude discs, are analyzed as well as discs with torque, the Joukowsky discs. The Froude disc is a Joukowsky disc with infinite rotational speed, but for analytical and historical reasons, it is treated as a stand-alone topic.

From Actuator Disc to Rotor Aerodynamics

The actuator disc is the basis for the industry standard rotor design method, the Blade Element Momentum (BEM) method. There is a good reason for this, as shown in Fig. 1. The black line gives the result of Froude's momentum theory, with the vertical axis showing the average velocity at the disc as a function of the non-dimensional thrust coefficient C_T. Added to this graph are results of experiments in the 1980s of the previous century, Anderson et al. (1982) and Wilmshurst et al. (1984); more recent experiments, Medici and Alfredsson (2006), Haans et al. (2008), Parra et al. (2016), and Lignarolo et al. (2016a); and calculations found in literature like Sørensen et al. (1998), Mikkelsen et al. (2009), and Madsen et al. (2010). The correspondence between the momentum theory and the data is quite good, except close to the maximum load on the actuator disc. Figure 1 also shows the engineering extension of the momentum theory for the heavily loaded disc developed by Glauert (1926) in the form presented by Hansen (2008).

The classical or Froude actuator disc momentum theory is not able to say anything about radial or azimuthal distributions of velocity and load for real rotors. The disc concept has been adapted by many as to make it useful for rotors with a finite number of blades. A major contribution was delivered by Glauert (1935, ch. III) who coupled disc loads to blade loads and introduced the torque in the momentum theory, resulting in the Blade Element Momentum method. One of the assumptions Glauert made to make the method executable is that the pressure in the far wake is uniform, despite the pressure gradient necessary to maintain swirl. Many authors have published similar adaptations with slightly different results, reviewed by Sørensen et al. (2015). The main problems that were left after Glauert's

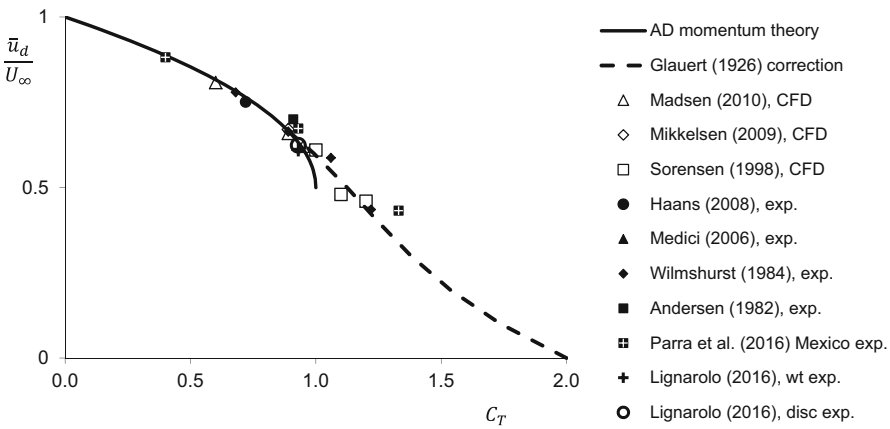

Fig. 1 Actuator disc momentum theory including an engineering extension compared with experiments and calculations for wind turbine flow states. The vertical axis shows the dimensionless velocity at the (rotor) disc, the horizontal axis the dimensionless thrust

work were the refinement of the blade model, the effect of swirl, the tip correction, the optimization procedure, and the adaptation of BEM to atmospheric and rotor conditions not covered by the first versions of BEM.

Force Fields in Rotor Aerodynamics

Rotor aerodynamics is one of the few areas in aerodynamics where force fields are used as input in flow calculations: the flow field induced by predefined forces is solved (the dynamic method). In most other aerodynamic analyses, the force field is the output instead of input: the flow field around a surface is solved using surface boundary conditions, after which the pressure and so the load are known (the kinematic method). One of the reasons why force fields as input are not used often is twofold: usually they are not known in advance, and the kinematic method for which Lanchester, Prandtl, and Joukowsky have laid the basis has been shown to be very powerful. However, the use of force fields has some advantages, especially for rotor aerodynamics since the thrust, being the integrated load, is the main parameter defining flow states.

Force Fields: Output from or Input in the Equation of Motion?

The use of force fields as input is common practice in classical actuator disc theory, in the momentum part of BEM methods, and in actuator line (AL) analyses. In the AL analyses, the blade is replaced by a load carrying line in order to have a much lower computation time compared to full computational fluid dynamic (CFD) solutions. The load in these methods is determined either by the definition of the problem (in actuator disc analyses, based on physical arguments a load distribution is assumed, e.g., Sørensen et al. 1998) or by iteration with other methods (in AL and momentum methods, for a given flow field, the load is taken from a blade element calculation, e.g., Shen et al. 2014). Besides its modest computational effort, the force field approach offers the advantage of a force field based interpretation of the three processes governing disc and rotor flows: the change of momentum, the generation or conservation of vorticity, and the conversion or conservation of energy, which are the topics of next sections.

Equivalence of the Kinematic and Dynamic Methods

Prandtl (1918) showed analytically that the pressure distribution acting on a translating lifting surface is equivalent to a distribution of normal forces acting on the surface modelled as a bound vortex sheet γ. In van Kuik (2018b) the equivalence of both approaches for the actuator disc and rotors is discussed in detail, including the comparison by Martínez-Tossas et al. (2017) of the flow around a Joukowsky

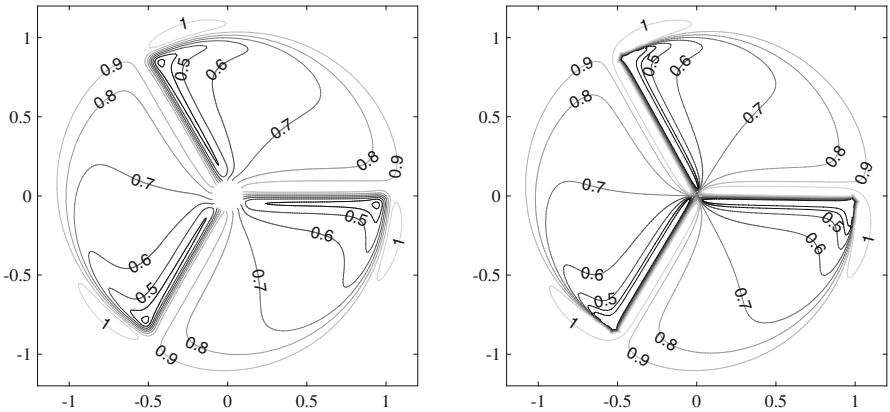

Fig. 2 Distribution of u/U_∞ at the rotor plane x $= 0$ according to the actuator line (left) and lifting line (right) model, for $\lambda = 7$ and $C_T = 8/9$, from van Kuik et al. (2015a). The direction of rotation is anti-clockwise

aerofoil modelled as a lifting surface and as a force distribution. Here a numerical comparison is shown in Fig. 2, where the axial velocity in the rotor plane of a three-bladed rotor with constant bound circulation is displayed, calculated by a lifting line (LL) method and an actuator line (AL) method as reported in van Kuik et al. (2015a). The LL method is the kinematic method: the blade is modelled as a line with prescribed constant bound circulation Γ. The AL method prescribes forces acting at the line. The force distribution is chosen such that the resulting circulation around the lines is identical to the prescribed constant circulation in the LL method. The load case shown is the wind turbine for tip speed ratio $\lambda = \Omega R/U_\infty = 7$ where Ω is the rotational speed of the force field. The thrust coefficient $C_T = T/\left(\frac{1}{2}\rho U_\infty^2 \pi R^2\right) = 8/9$. The results of both methods agree reasonably well except for minor differences for $r < 0.1R$ and near the tip, due to differences in the de-singularization of the vortices.

Sign Conventions. Figure 3 shows the coordinate systems. All vectors are drawn in positive direction, except Γ_{axis} and γ_φ. $\Delta H < 0$ as energy is taken from the flow. Consequently, power P and thrust T have a negative sign as these quantities refer to flow properties. As it is common to define power and thrust with respect to the disc, $P_{\text{disc}} = -P$ and $T_{\text{disc}} = -T$ are introduced. The power and thrust coefficients C_p and C_T are based on P_{disc} and T_{disc}, so are positive. The same holds for the power and thrust (coefficients) of the rotor. P, T, and all other quantities are defined as acting on the flow or as flow from properties.

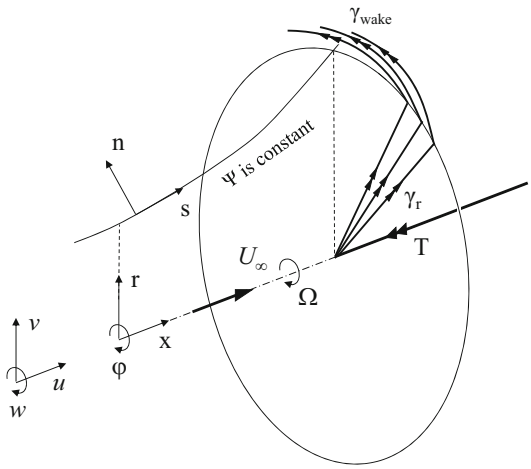

Fig. 3 The coordinate systems of an actuator disc and rotor. Ψ is the Stokes stream function, $u,\ v, and\ w$ are the axial, radial, and azimuthal velocity components. All vectors and components are in positive direction except Γ_{axis} and γ_φ

The Equation of Motion and the Coordinate Systems

The flow is assumed to be incompressible, steady, inviscid, and isentropic, so the Euler equation:

$$\rho\ (\boldsymbol{v} \cdot \nabla)\boldsymbol{v} = -\nabla p + \boldsymbol{f} \tag{1}$$

is valid as well as the continuity equation:

$$\nabla \cdot \boldsymbol{v} = 0, \tag{2}$$

with $\boldsymbol{v}$ being the velocity vector, ρ the flow density, p the pressure, and $\boldsymbol{f}$ the force density, volume force, or force field. All analyses assume steady flow, except for section "Non-conservative and Conservative Force Fields" where the work done by force fields is examined. The equation of motion then is $\rho\frac{\partial \boldsymbol{v}}{\partial t}+\rho(\boldsymbol{v}\cdot\nabla)\boldsymbol{v} = -\nabla p+\boldsymbol{f}$.

Rewriting (1) with the vector identity $(\boldsymbol{v} \cdot \nabla)\boldsymbol{v} = \nabla(\boldsymbol{v} \cdot \boldsymbol{v})/2 - \boldsymbol{v} \times \boldsymbol{\omega}$ yields:

$$\nabla H = \boldsymbol{f} + \rho\boldsymbol{v} \times \boldsymbol{\omega}, \tag{3}$$

where H is the Bernoulli constant $p+\frac{1}{2}\rho\boldsymbol{v}\cdot\boldsymbol{v}$ and $\boldsymbol{\omega}$ the vorticity. Most textbooks pay some attention to the force term but at some moment assume that $\boldsymbol{f}$ is conservative, like the gravity force field $\rho\boldsymbol{g}$. Then $\boldsymbol{f} = \rho\boldsymbol{g} = -\nabla\mathcal{G}$ where $\mathcal{G}$ is the potential of $\rho\boldsymbol{g}$. The right-hand side of (1) then becomes $-\nabla(p+\mathcal{G})$. With the potential $\mathcal{G}$ considered to be part of the pressure, the conservative $\boldsymbol{f}$ disappears from the equation of motion. Here this assumption is not made. Instead, force fields are assumed to be confined to thin surfaces having thickness ϵ; see Fig. 4. Integration of $\boldsymbol{f}$ along the normal n, becoming a Dirac delta function for $\epsilon \to 0$, gives the surface load $\boldsymbol{F}$:

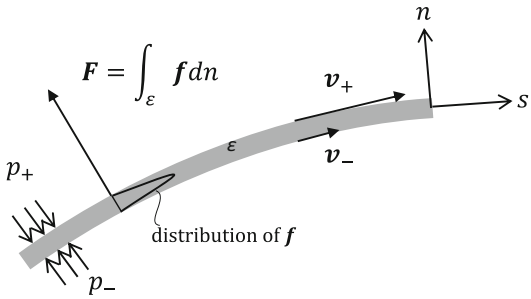

Fig. 4 Properties of a bound vortex sheet with thickness ϵ and force density distribution $\boldsymbol{f}$: pressure jump $p_- - p_+ = F_n$, velocity jump $|\boldsymbol{v}|_- - |\boldsymbol{v}|_+ = \gamma$

$$\boldsymbol{F} = \int_{\epsilon} \boldsymbol{f}\, dn. \tag{4}$$

More integrations result in a line force or a discrete force, which will be named after its function, e.g., lift or thrust.

Most analyses in this chapter use the cylindrical coordinate system $(x,\ r,\ \varphi)$ with the disc centerline coinciding with the positive x-axis and with $\boldsymbol{e}$ denoting the unit vector with an appropriate index. The corresponding components of the velocity vectors $\boldsymbol{v}$ are $u,\ v$, and w. The local coordinate system $(s,\ n,\ \varphi)$ is also shown in Fig. 3. The coordinates s and n are in the meridian plane tangent respectively normal to a streamline, with velocity components $v_s,\ v_n$, and w. Besides these inertial coordinate systems, also the rotating system $(x,\ r,\ \varphi)_{\text{rot}}$ is used, rotating with respect to the inertial system with the angular velocity Ω of the force field. The velocity and vorticity in the inertial and rotating systems are related by:

$$\boldsymbol{v}_{\text{rot}} = \boldsymbol{v} - \boldsymbol{e}_{\varphi}\Omega r \tag{5}$$

$$\boldsymbol{\omega}_{\text{rot}} = \boldsymbol{\omega} - 2\boldsymbol{e}_x\Omega. \tag{6}$$

Batchelor (1970, eq. (3.5.20)) gives the steady Euler equation in the rotating coordinate system, including the centrifugal force $-\boldsymbol{\Omega} \times (\boldsymbol{\Omega} \times \boldsymbol{r}) = \boldsymbol{e}_r\Omega^2 r = \frac{1}{2}\nabla(\Omega r)^2$ and Coriolis force $\boldsymbol{v}_{\text{rot}} \times 2\boldsymbol{\Omega}$ (note that Batchelor's equation (3.5.20) is without $\boldsymbol{f}$ and with the centrifugal term $\frac{1}{2}\nabla(\Omega r)^2$ included in ∇H). In the notation used here, this Euler equation becomes:

$$\boldsymbol{f} + \frac{\rho}{2}\nabla(\Omega r)^2 + \rho\boldsymbol{v}_{\text{rot}} \times 2\boldsymbol{\Omega} = \nabla H_{\text{rot}} - \rho\boldsymbol{v}_{\text{rot}} \times \boldsymbol{\omega}_{\text{rot}}. \tag{7}$$

With $\nabla H_{\text{rot}} = \nabla\left(H - \rho w\Omega r + \frac{\rho}{2}(\Omega r)^2\right)$ and with (6), this becomes:

$$\boldsymbol{f} = \nabla(H - \rho w\Omega r) - \rho\boldsymbol{v}_{\text{rot}} \times \boldsymbol{\omega}. \tag{8}$$

At those parts of the flow field where $\boldsymbol{\omega}$ and $\boldsymbol{f}$ are zero, this becomes:

$$\nabla(H - \rho w \Omega r) = 0, \tag{9}$$

which has been derived previously by Thwaites (1960, p. 473) and de Vries (1979, app. C2).

Non-conservative and Conservative Force Fields

The use of the force field $\boldsymbol{f}$ is discussed in old textbooks and papers, like Prandtl (1918) and von Kármán (1935), without making an explicit distinction between conservative and non-conservative components. In general, the force field can have both components:

A non-conservative force field is defined by:

$$\nabla \times \boldsymbol{f} \neq 0, \tag{10}$$

and is able to generate vorticity as shown by the curl of (3) (see Saffman 1992, pp. 10–11):

$$\frac{1}{\rho}\nabla \times \boldsymbol{f} = \frac{D\boldsymbol{\omega}}{Dt} - (\boldsymbol{\omega} \cdot \nabla)\, \boldsymbol{v}, \tag{11}$$

with the last term denoting the change of vorticity due to stretching or tilting of already-existing vortex filaments. When $\boldsymbol{f}$ is distributed on a surface with thickness ϵ as shown in Fig. 4, integration of $\nabla \times \boldsymbol{f}$ and taking the limit for $\epsilon \to 0$ gives:

$$\frac{1}{\rho}\nabla \times \boldsymbol{F} = \frac{D\gamma}{Dt} - (\boldsymbol{\gamma} \cdot \nabla)\, \boldsymbol{v}. \tag{12}$$

For inviscid flow around a 2-D aerofoil $\oint \nabla \times \boldsymbol{F} ds = 0$ with s taken along the aerofoil contour, as the integrand contains the derivative of the normal load, so the contour integral yields 0. Consequently, the force field is conservative and no vorticity is produced.

The force field of a 3-D lifting wing is non-conservative, producing trailing vorticity according to (12) when integrated over a half wing. However, when integrated over the entire surface S of a wing (or rotor blade):

$$\int_S \nabla \times \boldsymbol{F} dS = 0, \tag{13}$$

since the closed contour integration of the directional derivatives of the normal load yields 0. The force field of a lifting surface generates vorticity locally, but as an equal amount of opposite sign is produced somewhere else at the surface, the nett generation is zero. This is the force field based explanation of the fact that any lifting

surface with finite dimensions produces the same amount of positive and negative vorticity.

A conservative force field satisfies $\nabla \times \boldsymbol{f} = 0$ or, equivalently:

$$\boldsymbol{f} = -\nabla \mathcal{F} \tag{14}$$

where $\mathcal{F}$ is the potential of $\boldsymbol{f}$. With (14) the Euler equation (1) becomes:

$$\rho\ (\boldsymbol{v} \cdot \nabla)\boldsymbol{v} = -\nabla(p + \mathcal{F}). \tag{15}$$

When only conservative forces act, the flow is free of vorticity, so (3) becomes the Bernoulli equation:

$$\nabla(H + \mathcal{F}) = 0. \tag{16}$$

The quantity $(H + \mathcal{F})$ indicates the amount of energy per unit of mass as becomes clear by evaluation of the work done per second by force fields.

The work done by a force field is given by $\boldsymbol{f} \cdot \boldsymbol{v}$, according to Batchelor (1970, p. 157)]. The unsteady Euler equation $\boldsymbol{f} \cdot \boldsymbol{v} = \boldsymbol{v} \cdot \nabla H + \rho \boldsymbol{v} \cdot \partial \boldsymbol{v}/\partial t$ is used. Assuming a control volume V with surface S encompassing a distribution of steady or steadily rotating forces as shown in Fig. 7, the kinetic energy within the control volume remains constant, so the term $\int \frac{\rho}{2} \frac{\partial |\boldsymbol{v}^2|}{\partial t} dV = 0$. The result is:

$$\int_V \boldsymbol{f} \cdot \boldsymbol{v} dV = \int_V \boldsymbol{v} \cdot \nabla H dV = \int_S H v_{n,S} dS, \tag{17}$$

where $v_{n,S}$ is the velocity component normal to S having radius R_S and where Gauss's theorem is used to convert the volume integral into a surface integral. When $\boldsymbol{f}$ is conservative, the flow is free of vorticity, so for $R_S \to \infty$, $H_S \to H_\infty$. Then (17) becomes:

$$\int_V \boldsymbol{f}_{\text{cons}} \cdot \boldsymbol{v} dV = H_\infty \int_S v_{n,S} dS = 0. \tag{18}$$

This shows that $\boldsymbol{f}_{\text{cons}} \perp \boldsymbol{v}$: conservative forces cannot perform work; only non-conservative forces can. This specific property will be used in the momentum theory in sections "Analysis of Froude Actuator Disc Flows" and "Analysis of Joukowsky Actuator Disc Flows". Forces which do not appear in the energy balance while contributing to the momentum balance are classified as conservative.

The Disc as Representation of a Rotor

The actuator disc is the result of a limit transition of a rotor for an increasing number of blades. The formal limit transition is shown in van (van Kuik 2018b, section 4.3), while here the equivalence of the expressions for thrust and power is treated. Lignarolo et al. (2016a, b) have compared the wake behind a disc and model rotor, having the same size and measured in the same wind tunnel. The experiments have confirmed that the disc wake is a true representation of the azimuthally averaged wake of a wind turbine rotor

The Actuator Disc Equation

As only the pressure and azimuthal velocity will be discontinuous across the infinitely thin disc, integration of (1) across the disc gives:

$$\boldsymbol{F} = \boldsymbol{e}_x \Delta p + \boldsymbol{e}_\varphi \rho u \Delta w, \tag{19}$$

where Δ denotes the jump across the disc. The Bernoulli equation $p + \frac{1}{2}\rho \boldsymbol{v} \cdot \boldsymbol{v} = H$, integrated across the disc, becomes:

$$F_x = \Delta p = \Delta H - \frac{1}{2}\rho \Delta w^2. \tag{20}$$

The power produced or absorbed by an annulus dr of the actuator disc can be expressed in two ways: first as torque Q times rotational speed Ω giving $\Omega dQ = 2\pi \Omega f_\varphi r^2 dr$ and second by integration of $\boldsymbol{f} \cdot \boldsymbol{v}$ using (3), resulting in $2\pi r(\boldsymbol{v} \cdot \nabla) H dr$. Comparison shows that:

$$\boldsymbol{f} \cdot \boldsymbol{v} = \Omega r \, f_\varphi = (\boldsymbol{v}.\nabla) H. \tag{21}$$

The expression for f_φ is derived from the φ-component of (1), with $(\boldsymbol{v}.\nabla)\boldsymbol{v}$ evaluated in the cylindrical coordinate system:

$$r f_\varphi = \rho (\boldsymbol{v} \cdot \nabla) r w. \tag{22}$$

Substitution in (21) gives:

$$\boldsymbol{f} \cdot \boldsymbol{v} = \rho (\boldsymbol{v}.\nabla)(\Omega r w) = (\boldsymbol{v}.\nabla) H, \tag{23}$$

so:

$$\frac{1}{\rho} \nabla H = \nabla (\Omega r w). \tag{24}$$

This is the same equation as (9) but now without the restriction that $\boldsymbol{f}$ and $\boldsymbol{\omega}$ are absent.

Equation (24) shows that the work done by the force field is expressed in a change of the Bernoulli constant H. Integrated across the disc, this gives:

$$\Delta H = \rho \Omega r w. \tag{25}$$

Combined with (20):

$$F_x = \rho \Omega r w - \frac{1}{2} \rho w^2. \tag{26}$$

Both terms at the right-hand side are pressure jumps: $\Delta p_H = \rho \Omega r w$ converts power so is non-conservative, while the pressure jump $\Delta p_w = -\frac{1}{2}\rho w^2$ is balanced by an equal increase of kinetic energy, $\frac{1}{2}\rho w^2$. Δp_w is the change of potential energy which, in combination with the change of kinetic energy, does not change H, so is conservative.

A combination of (24) with (8) gives:

$$\boldsymbol{f} = -\rho \boldsymbol{v}_{\text{rot}} \times \boldsymbol{\omega}. \tag{27}$$

An alternative way to derive (27) is to express (24) in $\boldsymbol{\omega}$: $\frac{1}{\rho}\nabla H = \nabla(\Omega r w) = \boldsymbol{e}_\varphi \Omega r \times \boldsymbol{\omega}$. Substitution in the Euler equation (3) using the coordinate transformations (5) and (6) results in (27). With ϵ denoting the thickness of the disc, integration across the disc and taking the limit $\epsilon \to 0$ gives:

$$\boldsymbol{F} = -\rho \int_\epsilon \boldsymbol{v}_{\text{rot}} \times \boldsymbol{\omega} d\epsilon = -\rho \bar{\boldsymbol{v}}_{\text{rot}} \times \boldsymbol{\gamma}_d. \tag{28}$$

where $\bar{\boldsymbol{v}}_{\text{rot}}$ is the average of $\boldsymbol{v}_{\text{rot}}$ upstream and downstream of the disc.

Equation (28) is the equation of motion for the steady actuator disc converting power for any radial distribution of $\boldsymbol{F}$. The subscript $_{\text{rot}}$ in (28) distinguishes it from the expression of a Kutta-Joukowsky force: the disc load is the cross product of the velocity as experienced in the rotating system with the vorticity in the inertial system. Since it is expressed in kinematic terms, it enables an easier physical interpretation of the relation between loads and vorticity compared to the Euler equation including H.

Equation (28) is comparable with the expression for the load on a rotor blade. Figure 6 shows a blade having a cross section C at which the bound vorticity is distributed. The sectional load on a blade is:

$$\boldsymbol{L} = -\rho \int_C \boldsymbol{v}_{\text{rot}} \times \boldsymbol{\omega} dC. \tag{29}$$

Depending on the orientation of $\boldsymbol{v}_{\text{rot}}$ and $\boldsymbol{\omega}$, the sectional load may have a radial component, besides the axial and azimuthal components. Figure 6 shows the load on the radial bound vorticity but also, close to the blade tip and root, on the chordwise bound vorticity, being able to carry an additional axial and radial load. This is treated in detail in van Kuik (2018b). In case the blade is modelled as a lifting line, so $C \to 0$, only the radial bound vorticity is maintained, and:

$$\lim_{c \to 0} \boldsymbol{L} = -\rho \int_C \boldsymbol{v}_{\text{rot}} \times \boldsymbol{e}_r \omega_r dC = -\rho \boldsymbol{v}_{\text{rot,B}} \times \boldsymbol{\Gamma}_B \tag{30}$$

with the blade vortex strength $\boldsymbol{\Gamma}_B = \boldsymbol{e}_r \int_C \omega_r dC$ remaining invariant for $C \to 0$ and with $\boldsymbol{v}_{rot,B}$ the velocity at the position of the lifting line. Equation (30) is similar to (28), enabling a formal limit transition from rotor to disc as presented in van Kuik (2018b).

Power and Thrust Expressions of Joukowsky Discs and Rotors

Figure 5 shows the disc model of Joukowsky, characterized by a constant circulation Γ around the axis. The disc vorticity system has a centerline vortex Γ with core radius δ and disc vorticity $\gamma_d = -\Gamma/(2\pi r)$ for $r > \delta$. The azimuthal velocity w in the wake depends only on Γ. Inside the core, w depends on the assumed characteristics of the core. The force field rotates with angular velocity Ω. A Joukowsky rotor is characterized by the same vortex at the axis which continues

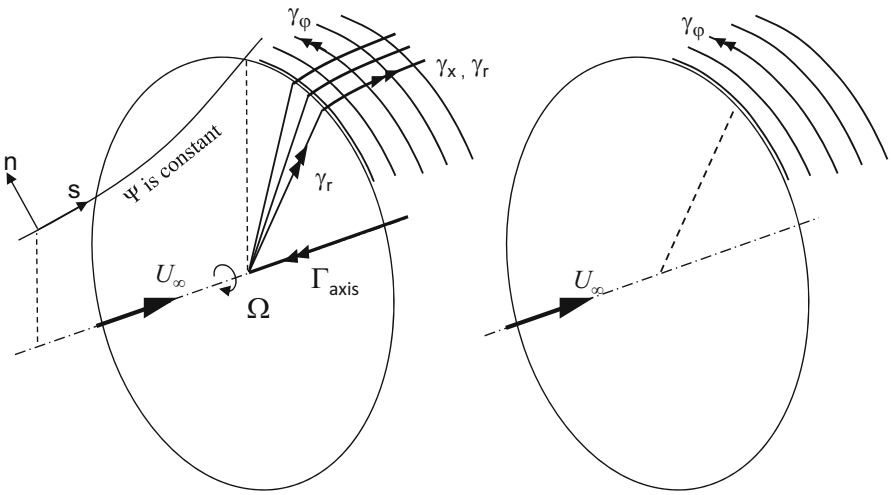

Fig. 5 The circulation distribution for the Joukowsky actuator disc with swirl, left, and the Froude disc without swirl, right

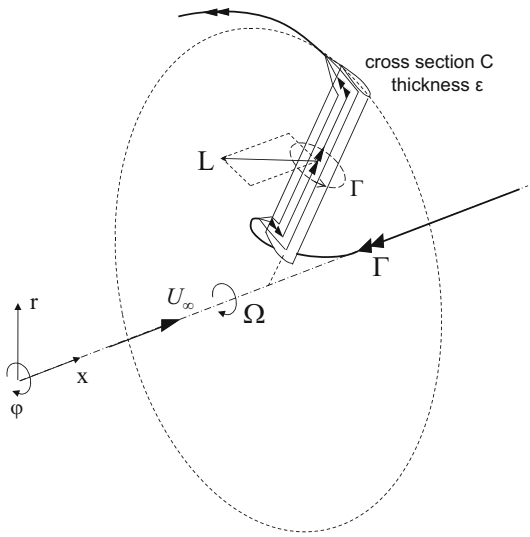

Fig. 6 The load on bound radial vorticity of a wind turbine rotor blade. Sign conventions are shown in Fig. 3. The number of blades is B, and $\Gamma_{\text{axis}} = -B\Gamma_B$

in a constant blade bound circulation, as shown in Fig. 6 for a one-bladed rotor. For a rotor with B blades $\Gamma_{\text{axis}} = -B\Gamma_B$.

The disc: The non-conservative force field of a steady actuator disc converts power as given by (17):

$$P = \int_V \boldsymbol{f} \cdot \boldsymbol{v} dV = \int_S H v_{n,S} dS \tag{31}$$

with volume V having surface S shown in Fig. 7. At the cross section with the far wake $v_{n,S} = u_1$. At the cross section with the stream tube far upstream, the velocity is undisturbed U_∞. For the part of V outside the stream tube, $H = H_\infty$ and $\int v_{n,S} dS = 0$, so the expression for the converted power becomes:

$$P = \int_{A_1} H\, u_1 d\, A_1 - H_\infty U_\infty A_\infty, \tag{32}$$

where A_∞ is the cross section of the stream tube far upstream and A_1 the same far downstream. For the Joukowsky disc, the azimuthal velocity is:

$$\left.\begin{aligned} w &= \frac{\Gamma}{2\pi r} && \text{for } r \geq \delta \\ &= \frac{\Gamma}{2\pi\delta} \mathcal{C}\left(\frac{r}{\delta}\right) && \text{for } r < \delta \end{aligned}\right\} \tag{33}$$

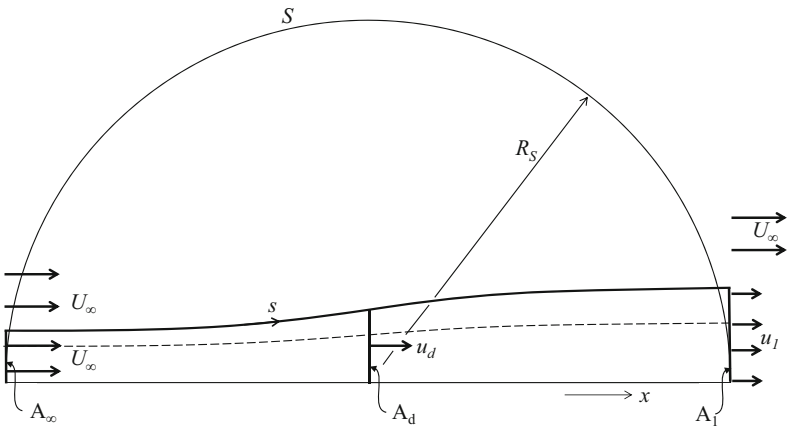

Fig. 7 Half-sphere with surface S as control volume for the momentum balance, crossing the stream tube of an actuator disc far upstream with undisturbed flow and far downstream with a fully developed wake. Only half of the cross section is displayed

where $\mathcal{C}(1) = 1$ and $\mathcal{C}(0) = 0$ but otherwise unspecified. As an example, with $\mathcal{C}(r/\delta) = r/\delta$, the vortex core is modelled as a Rankine vortex. With (24) it follows that:

$$\left.\begin{aligned} \frac{1}{\rho}(H - H_\infty) &= \frac{\Omega\Gamma}{2\pi} && \text{for } r \geq \delta \\ &= \frac{\Omega\Gamma}{2\pi}\frac{r}{\delta}\mathcal{C}\left(\frac{r}{\delta}\right) && \text{for } r < \delta \end{aligned}\right\} \tag{34}$$

Outside the core H is constant, so the power becomes:

$$P = \rho\Omega\Gamma\int_0^{R_1} u_1 r_1 dr_1 = \rho\frac{\Omega\Gamma}{2}\overline{u_d}R^2 \quad \text{for a J-disc, } \delta \to 0, \tag{35}$$

where conservation of mass $U_\infty A_\infty = u_1 A_1 = \overline{u_d}A_d$ is used to express the last term at the right-hand side of (32) in far wake properties and to convert the integral from plane A_1 to the disc area, with $\overline{u_d}$ being the disc averaged axial velocity. For $r < \delta$, integration of $u_1(H - H_\infty)$ across the vortex core cross section and letting $\delta \to 0$ shows that the contribution of the vortex core to P vanishes. This is checked by modelling $\mathcal{C}$ as a series development in $(r/\delta)^n$, showing that each term yields a zero contribution after integration across the core cross section.

With the introduction of the non-dimensional vortex strength $q = \Gamma/(2\pi RU_\infty)$ and tip speed ratio $\lambda = \Omega R/U_\infty$, (34) becomes for $r \geq \delta$:

$$\frac{\Delta H}{\rho U_\infty^2} = q\lambda \quad \text{for} \quad r \geq \delta. \tag{36}$$

Herewith the dimensionless power coefficient C_p becomes, with $P_{\text{disc}} = -P$ as explained in the text box *Sign Conventions* at page 4:

$$C_p = \frac{P_{\text{disc}}}{\frac{1}{2}\rho U_\infty^3 \pi R^2} = -2q\lambda \frac{\overline{u_d}}{U_\infty} \text{ for a J-disc, } \delta \to 0. \tag{37}$$

The thrust T is obtained by integration of (26) on the disc area. With (33) the contribution by the region outside the vortex core in the limit $\delta \to 0$ becomes:

$$T|_{\delta \leq r \leq R} = \rho\pi \int_\delta^R (2\Omega r^2 w - w^2 r)\, dr = \rho \frac{\Omega\Gamma}{2} R^2 - \rho \frac{\Gamma^2}{4\pi} \ln\left(\frac{R}{\delta}\right) \text{ for a J-disc, } \delta \to 0 \tag{38}$$

In the same way, the contribution to the thrust by the vortex core cross section is found to be a constant, like $-\rho\frac{\pi}{4}(\frac{\Gamma}{2\pi})^2$ in case of the Rankine distribution $\mathcal{C}(r/\delta) = r/\delta$. For $\delta \to 0$ these constants vanish compared to the singular term in (38), so the thrust is:

$$T = \rho \frac{\Omega\Gamma}{2} R^2 - \frac{\rho}{2}\pi \left(\frac{\Gamma}{2\pi}\right)^2 \ln\left(\frac{R}{\delta}\right)^2 \text{ for a J-disc, } \delta \to 0. \tag{39}$$

The first term at the right-hand side is the thrust converting power. The second term is the thrust due to the swirl-induced pressure gradient. In dimensionless notation, the thrust coefficient becomes:

$$\left.\begin{aligned} C_T &= \frac{T_{\text{disc}}}{\frac{1}{2}\rho U_\infty^2 \pi R^2} \\ C_{T,\Delta H} &= -2\lambda q \\ C_{T,\Delta w} &= q^2 \ln\left(\frac{R}{\delta}\right)^2 \end{aligned}\right\} \text{J-disc, } \delta \to 0 \tag{40}$$

which is independent from the choice of the vortex core model. For $\delta \to 0$, $C_{T,\Delta w} \to \infty$. The consequences of this will be discussed at the end of this section.

ΔH is proportional to $\Omega\Gamma$, so with ΔH kept constant, w vanishes like Ω^{-1} as well as γ_d and Γ when $\Omega \to \infty$. The disc without swirl is the Froude actuator disc; see Fig. 5.

The rotor with B blades: The converted power P is torque Q times Ω, so with the azimuthal component of (30):

$$P = Q\Omega = -\Omega B\rho \int_{\delta}^{R} \int_{C} u\omega_r r dr dC. \tag{41}$$

In (30) the limit $C \to 0$ was included, leading to $\int_C u\omega_r dC = u_B \Gamma_B$. As before $\Gamma = -B\Gamma_B$, yielding:

$$P = \rho\Omega\Gamma \int_{\delta}^{R} u_B r dr \text{ for a J-rotor, } \delta \to 0, \tag{42}$$

so the power coefficient becomes:

$$C_p = -2\lambda q \overline{\frac{u_B}{U_\infty}} \text{ for a J-rotor, } \delta \to 0. \tag{43}$$

The thrust at the rotor is defined by the axial component of (30). With (5) and with $\Gamma = -B\Gamma_B$:

$$T = -\rho\Gamma \int_{\delta}^{R} w_{\text{rot},B} dr = \rho \frac{\Omega\Gamma}{2} R^2 - \rho\Gamma \int_{\delta}^{R} w_B dr \text{ for a J-rotor, } \delta \to 0. \tag{44}$$

In the wake the azimuthally averaged value $\bar{w} = \Gamma/(2\pi r)$, but in the rotor plane, it is half this value: $\overline{w_{x=0}} = \Gamma/(4\pi r)$. The azimuthal distribution of w will be approximately uniform for low values of r/R as the induction by the root vortex dominates. However, for larger r/R values, the tip vortices will add a harmonic distribution. With the actuator line and lifting line calculations of which the axial velocity is shown in Fig. 2, the order of magnitude of the approximation $w_B = \bar{w}$ is estimated: the deviation in C_T is <0.1%, so the approximation is well in place.

When the non-uniformity of w is neglected $w_B/U_\infty \approx \Gamma/(4\pi r U_\infty)$ for $r > \delta$, so the result for C_T is, with again $C_T = C_{T,\Delta H} + C_{T,\Delta w}$:

$$\left.\begin{aligned} C_T &= \frac{T_{\text{rotor}}}{\frac{1}{2}\rho U_\infty^2 \pi R^2} \\ C_{T,\Delta H} &= -2\lambda q \\ C_{T,\Delta w} &= 4q \int_{\delta}^{R} \frac{w_B}{U_\infty R} dr \\ &\approx q^2 \ln\left(\tfrac{R}{\delta}\right)^2 \end{aligned}\right\} \text{J-rotor, } \delta \to 0. \tag{45}$$

The local thrust coefficient C_t is defined as $BdL_x/(\rho U_\infty^2 \pi r dr)$, where L_x is the axial component of (30):

$$C_t = -2\lambda q + 2q\frac{w_B}{U_\infty}\frac{R}{r}, \text{ for a J-rotor, } r \geq \delta, \tag{46}$$

or, with $C_t = C_{t,\Delta H} + C_{t,\Delta w}$:

$$\left.\begin{aligned} C_{t,\Delta H} &= -2\lambda q \\ C_{t,\Delta w} &= 2q\frac{w_B}{U_\infty}\frac{R}{r} \\ &\approx q^2\left(\frac{R}{r}\right)^2 \end{aligned}\right\} \text{J-rotor, } \delta \to 0. \tag{47}$$

The expressions for the rotor and disc are identical, apart from the approximation in (45) and (47) for the rotor thrust component $C_{T,\Delta w}$. For the disc as well as rotor, the conversion of power by the force field is expressed in the increase of the amount of wake swirl.

$C_{T,\Delta w}$ becomes ∞ for $\delta \to 0$ as long as q^2 is non-zero. This is the case for finite Ω when ΔH or $q\lambda$ remains constant in this limit. With $\delta \ll R$ the singular term is positive, so it adds up to $C_{T,\Delta H}$ for a wind turbine rotor. For practical conditions δ mimics the root cut-out radius, which is the radius below which the nacelle and blade root connection occupy the space. A practical value is $0.15R$. For $\lambda > 7$ we find that $C_{T,\Delta w} \leq 0.02C_{T,\Delta H}$, so this contribution to the thrust may be ignored. In section "Analysis of Joukowsky Actuator Disc Flows" $C_{T,\Delta H}$ will be used as parameter defining flow states, together with λ. The unknown in the power coefficient C_P is $\bar{u}_d$ for the disc and $\bar{u}_B$ for the rotor. The determination of $\bar{u}_d$ is the topic of the following sections.

Analysis of Froude Actuator Disc Flows

This actuator disc momentum theory for Froude discs, so discs without swirl, is sometimes called "one-dimensional" as only the axial momentum balance is included. It is a special case of Joukowsky discs as it results from the limit $\Omega \to \infty$. However, in accordance with its place in the history of rotor aerodynamics, it is treated first as an independent topic. The theory gives the average value of the axial velocity at the disc, not the velocity distribution. Modern computational approaches are able to provide flow details like the shape and strength of the vortex tube that separates the wake from the outer flow. Using a CFD solver for the Navier-Stokes equations, the velocity field for propeller as well as wind turbine flows states was first published by Sørensen et al. (1998). The method to find details of the actuator disc flow used in this chapter is based on the inviscid method of Øye (1990). The method is described in van Kuik and Lignarolo (2016) and van Kuik (2018a).

The Momentum Balance

The general expression for the momentum balance is given by Batchelor (1970, p. 138). For inviscid flow the balance in x-direction drawn on a volume V enclosed by a surface S is:

$$T - \oint_S \boldsymbol{e_x} \cdot \boldsymbol{e_n} p dS = \rho \oint_S u(u - U_\infty) dS \tag{48}$$

with p being the pressure acting at the boundary S. When applied to the stream tube passing through the disc, the pressure integral becomes zero, as will be shown. Section "Momentum Theory Including Conservative Forces" treats the balance of an annulus instead of the entire stream tube, where the annulus-based pressure integral will be shown to be non-zero.

Usually the stream tube passing through the actuator is used as the control volume V. Several proofs have been published that the pressure acting at the stream tube boundary does not contribute to the momentum balance, e.g., by Thoma (1925). Here another control volume is used. Figure 7 shows the control volume bounded by a sphere with radius R_S, with the center of the sphere coinciding with the center of the actuator disc, and with $R_S \to \infty$. The advantage of this control volume is that only the flow conditions at infinite distance need to be known, not at the vortex sheet itself. Furthermore this control volume can be used for the flow induced by a static disc ($U_\infty = 0$) which does not have a stream tube extending upstream.

Outside the wake of the actuator disc at a large distance from the origin, the flow can be considered as a summation of a parallel flow and a source flow. Analogous to Batchelor (1970, p. 351), momentum and pressure terms in (48) at the sphere S but outside the wake vanish for $R_S \to \infty$. This is because the summation of undisturbed U_∞ and source-induced velocities $\boldsymbol{v}_{\text{source}}$ gives rise to momentum flux and pressure terms containing U_∞^2, $u_{\text{source}} U_\infty$, $v_{\text{source}} U_\infty$, and $|\boldsymbol{v}|^2_{\text{source}}$. The source velocity vanishes like R_S^{-2} by continuity of mass, so the $|\boldsymbol{v}|^2_{\text{source}}$ term does not contribute after integration on S for $R_S \to \infty$. The mixed terms containing $u_{\text{source}} U_\infty$, $v_{\text{source}} U_\infty$ do not vanish for increasing R_S but do not contribute after integration on S, due to the symmetry of the source flow with respect to the plane $x = 0$. The same holds for the constant term containing U_∞^2. What remains for $R_S \to \infty$ are the contributions by the disc itself and the momentum transport at stream tube cross sections A_∞ far upstream and A_1 far downstream. The pressure acting at these cross sections is undisturbed, p_∞, so the pressure integral in (48) vanishes and the momentum balance becomes:

$$T = \rho \int_{A_1} u_1 (u_1 - U_\infty) dA_1. \tag{49}$$

The same result is obtained when we use the stream tube as control volume and assume that the pressure $(p - p_\infty)$ at the stream tube boundary does not result

in an axial force acting on the control volume. In other words, the momentum balance using the sphere as control volume confirms this assumption, so it may be considered as an indirect proof that the stream tube pressure does not contribute.

Momentum Theory Without Conservative Forces

The Bernoulli equation applied to the upstream and downstream part of a streamline (the dashed line in Fig. 7) can be coupled by the pressure jump Δp, giving the energy balance:

$$\Delta p = \frac{1}{2}\rho(u_1^2 - U_\infty^2). \tag{50}$$

As Δp is uniform for Froude discs; also the velocity in the wake u_1 is uniform. With $T = \Delta p A_d$ the momentum balance (49) becomes:

$$\Delta p A_d = \rho u_1(u_1 - U_\infty)A_1 = \rho \bar{u}_d(u_1 - U_\infty)A_d, \tag{51}$$

where mass conservation $\overline{u_d}A_d = u_1 A_1$ is used and where $\overline{u_d}$ is the velocity averaged on the disc area. Elimination of Δp from (50) and (51) gives the famous result, first obtained by Froude (1889):

$$\overline{u_d} = \frac{1}{2}(u_1 + U_\infty). \tag{52}$$

The converted power $P = \Delta p \overline{u_d} A_d$, so in dimensionless form the power coefficient is, with $P_{\text{disc}} = -P$:

$$C_p = \frac{P_{\text{disc}}}{\frac{1}{2}\rho U_\infty^3 A_d} = -\frac{1}{2}\left(\left(\frac{u_1}{U_\infty}\right)^2 - 2\right)\left(\frac{u_1}{U_\infty} + 1\right). \tag{53}$$

The thrust coefficient follows by (50):

$$C_T = \frac{T_{\text{disc}}}{\frac{1}{2}\rho U_\infty^2 A_d} = 1 - \left(\frac{u_1}{U_\infty}\right)^2. \tag{54}$$

Expressed in $\overline{u_d}$ both coefficients become:

$$C_p = -4\left(\frac{\overline{u_d}}{U_\infty}\right)^2\left(\frac{\overline{u_d}}{U_\infty} - 1\right) \tag{55}$$

and:

$$C_T = -4\frac{\overline{u_d}}{U_\infty}\left(\frac{\overline{u_d}}{U_\infty} - 1\right). \tag{56}$$

Elimination of $\overline{u_d}$ from (55) and (56) gives:

$$C_p = \frac{1}{2}C_T\left(1 + \sqrt{1 - C_T}\right), \tag{57}$$

which is the solid line in Figs. 1 and 9. Differentiation of (55) to $\overline{u_d}$ to find the coefficient for maximum power extraction gives:

$$C_{p,\max} = \frac{16}{27} \text{ for } \frac{\overline{u_d}}{U_\infty} = \frac{2}{3}, C_T = \frac{8}{9}, \tag{58}$$

which was obtained by Joukowsky (1920) and Betz (1920), for which reason it is called the Betz-Joukowsky maximum; see Okulov and van Kuik (2012).

Momentum Theory Including Conservative Forces

In the previous section, the momentum balance is applied to the entire stream tube, with the non-conservative disc load $T_{\text{non-cons}} = \Delta p A_d$ as the only load entering this balance. Now it is assumed that conservative loads are present in case the pressure integral in (48): $T_{\text{cons}} = -\oint_S \boldsymbol{e_x} \cdot \boldsymbol{e_n} p dS \neq 0$. Herewith the momentum balance becomes:

$$T_{\text{non-cons}} + T_{\text{cons}} = \rho \oint_S u(u - U_\infty) dS \tag{59}$$

with:

$$\left.\begin{aligned} T_{\text{non-cons}} &= \Delta p A \\ T_{\text{cons}} &= -\oint_S \boldsymbol{e_x} \boldsymbol{e_n} p dS. \end{aligned}\right\} \tag{60}$$

The energy equation (50) is unaffected by T_{cons} so the combination of (59) with (51) gives:

$$\overline{u_d} = \left(\frac{T_{\text{cons}}}{T_{\text{non-cons}}} + 1\right)\frac{U_\infty + u_1}{2}. \tag{61}$$

Expression (55) for the power coefficient becomes:

$$C_p = \left(\frac{T_{\text{cons}}}{T_{\text{non-cons}}} + 1\right) C_{p,T_{\text{cons}}=0} \tag{62}$$

and for the thrust coefficient:

$$C_T = C_{T_{\text{cons}}} + C_{T_{\text{non-cons}}} \tag{63}$$

Equations (61) and (62) have first been derived by van Holten (1981) for discs or rotors placed in a shroud or ring wing or with tip vanes. The lift on the additional device contributes to the momentum balance but does not convert energy, so is conservative. The average axial velocity at the disc is then given by (61). When both trust components have the same sign, the average velocity increases and so does the power coefficient. Sørensen et al. (2015, section 3.4) presents a survey of recent publications on the so-called diffuser-augmented wind turbines and discusses the associated momentum theory in detail. This theory is outside the scope of the present chapter.

Equation (61) has also been derived by Sørensen and Mikkelsen (2001) and is included in Sørensen and van Kuik (2011a) although they, as well as van Holten (1981), did not use the classification *cons* and $non - cons$. Sørensen and Mikkelsen (2001) derived (61) for the momentum theory applied to a stream annulus instead of stream tube. A stream annulus is a part of the stream tube, e.g., the volume bounded by the streamline shown as a dashed line in Fig. 7 or the volume between two such streamlines passing the disc at radii r and $r + \Delta r$ as shown in Fig. 8. The evaluation of (61) for an annulus as control volume will be done in section "The Momentum Balance Per Annulus".

Numerical Assessment of Actuator Disc Performance

In order to supplement the results of the momentum theory with flow details like the velocity and pressure distributions at the disc and in the wake, van Kuik and Lignarolo (2016) developed a numerical potential flow code which calculates the position and strength of the wake boundary for a prescribed uniform pressure jump Δp. With the wake vorticity known, all flow details can be calculated.

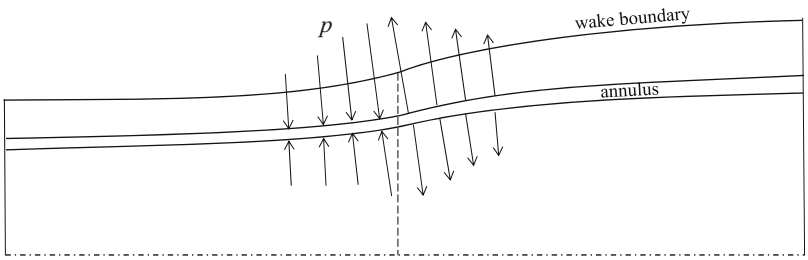

Fig. 8 The annulus as control volume for the momentum balance, including the contribution of the pressure at the surface of the annulus

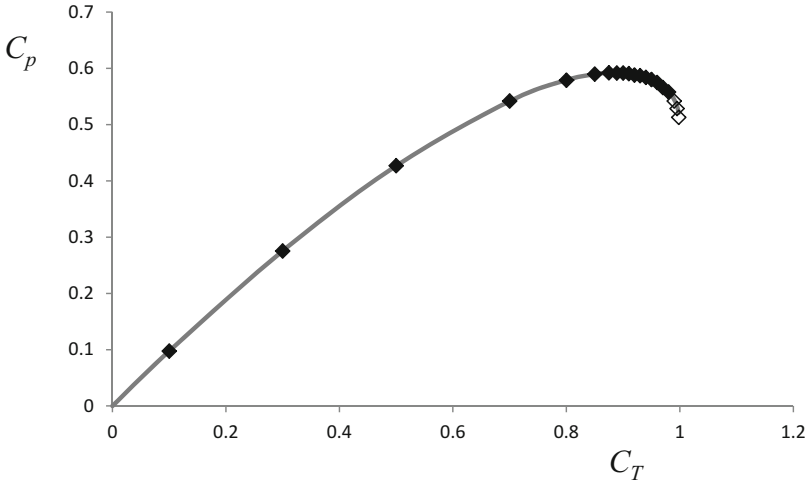

Fig. 9 Comparison of momentum theory (–) and computed C_p as a function of C_T. The data displayed by an open square do not have the required accuracy of maximal 0.3% deviation from momentum theory

Figure 9 shows the efficiency for wind turbine discs. The results of Froude's actuator disc momentum theory are reproduced accurately: for $C_T = 8/9$, R/R_1 deviates <0.1%, the induced velocity and C_p 0.25%, with the boundary conditions satisfied within 0.1%.

The code was validated by the actuator disc experiment of (Lignarolo et al. 2016b) providing the flow field as measured by stereo particle image velocimetry. The measured and calculated velocity vectors and wake expansion match well.

Flow and Pressure Patterns

Figure 10 shows the velocity vectors, streamlines, wake boundary, and isobars for $C_T = 8/9$. All other flow states show similar patterns. The isobars show a continuous pressure at the wake boundary but a discontinuous pressure gradient.

Properties of the Wake Boundary

A steady actuator disc with a uniform load $\boldsymbol{e}_x \Delta p$ creates a wake in which the Bernoulli constant is uniform, as follows from (3) which reduces in the wake to $\nabla H = 0$. Upstream of the disc and outside the wake also $\nabla H = 0$. The jump ΔH across the force free wake boundary is the same as the pressure jump across the disc. For the wake boundary ΔH becomes:

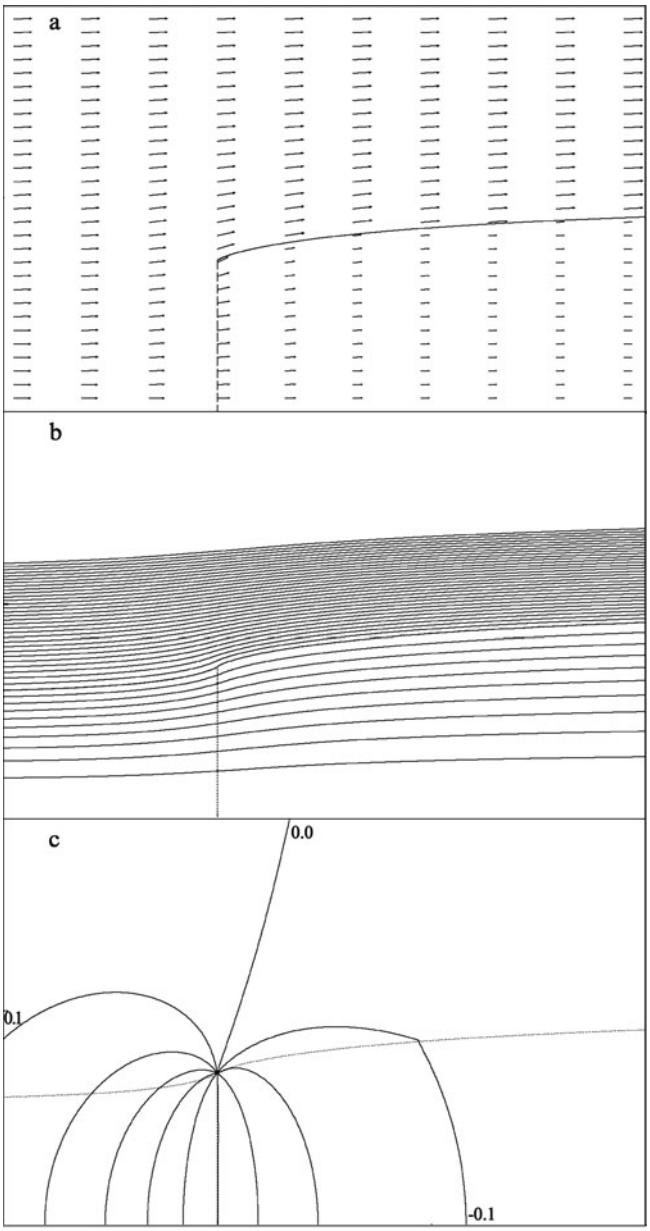

Fig. 10 For $C_T = 8/9$: (**a**) shows the velocity field and wake boundary, (**b**) stream tube value Ψ/Ψ_1, (**c**) isobars $(p - p_\infty)/|\Delta p|$, both with increments of 0.1. The isobar -0.4 almost coincides with the actuator disc

$$\Delta H = \Delta\left(\frac{1}{2}\rho|\boldsymbol{v}|^2\right). \tag{64}$$

With $\gamma = (v_- - v_+)$ denoting the strength of the vortex sheet, v_- and v_+ the velocities at the wake side and outer side of the sheet, and $v_s = \frac{1}{2}(v_- + v_+)$ the velocity of the sheet, (64) becomes:

$$\rho v_s \gamma = \Delta H = \text{constant}. \tag{65}$$

As γ and ΔH have a negative sign, this implies that the product $v_s\gamma$ is constant but < 0 along the vortex sheet. Figure 11 shows the calculated distribution $\gamma(s)$. For the flow case $C_T = 8/9$, the maximum of γ occurs at $s/R = 0.0513$. The distribution tends to become singular for $s/R \to 0$ with $d\gamma/ds > 0$ at $s = 0$. Using (65) this implies that v_s increases immediately after $s = 0$ reaching a maximum value at a small distance behind the disc, whereafter v_s decreases until $v_{s,1}$ is reached in the far wake. The strength of the vortex sheet seems to exhibit a singular behavior at the disc leading edge as shown in Fig. 11. For $s \to 0$ the strength $\gamma \to -\infty$, but as discussed in van Kuik (2018b), it is not possible to draw qualitative conclusions with respect to the singular behavior.

For all flow cases, the shape of the vortex sheet close to its leading edge is somewhat curved but does not show a particular behavior. The slope of the vortex sheet at $x = 0$ is always less than 90°, so the sheet does not turn upwind of $x = 0$. For $C_T = 0.998$ the slope is 65°; for $C_T = 8/9$ it is 46°.

Pressure at the Axis

Figure 12 shows the pressure distribution at the axis for $C_T = 8/9$. The pressure jump across the disc is not symmetric: $|(p - p_\infty)|_{\text{upstream}} \neq |(p - p_\infty)|_{\text{downstream}}$. A symmetric jump would require, by the Bernoulli equation, that at the axis of the disc $\frac{1}{2}\rho(u_{r=0}^2 - U_\infty^2)_{x=0} = \frac{1}{2}\Delta p$, leading to $u_{r=0}/U_\infty = 0.745$. This differs from the calculated value 0.685 shown in Fig. 13. Apart from this numerical disagreement, there is no argument found in the momentum theory why the pressure jump should be symmetric.

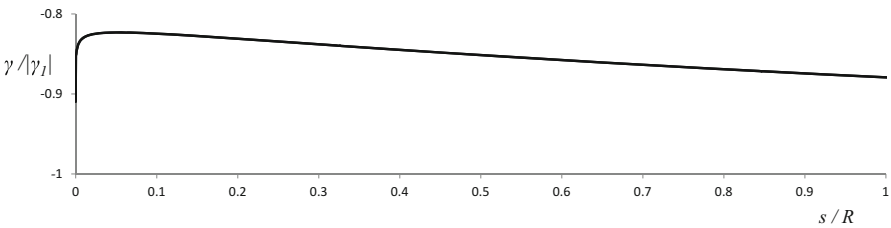

Fig. 11 The distribution of the vortex sheet strength $\gamma(s)$ as a function of the distance s/R measured along the sheet, for $C_T = 8/9$

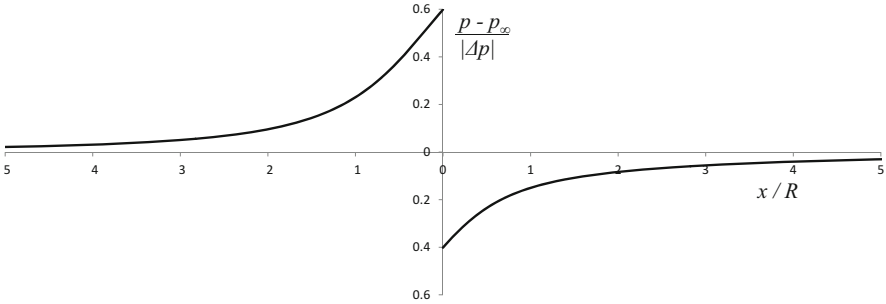

Fig. 12 The pressure distribution at the disc axis for $C_T = 8/9$

The Velocity Distribution at the Disc

The velocity components at the disc are presented in Fig. 13, showing that $|v|$ is constant (with a deviation of $\pm 0.2\%$) for $C_T = 8/9$. The same behavior is found for all other values of C_T. To explain this constant velocity, the radial component of the equation of motion (1) is helpful:

$$\rho v \frac{\partial v}{\partial s} = -\frac{\partial p}{\partial r}. \tag{66}$$

As the disc force field is only axial, f is absent in (66). When following a streamline passing the disc and observing the increase or decrease of v, it is clear that $\partial v/\partial s > 0$ when travelling from upstream infinity to the disc as the induction by the wake vorticity increases. After having passed the disc, the wake vorticity in between the disc and the downstream position of observation induces a negative v, contributing $\partial v/\partial s < 0$ for increasing s. The vortex tube downstream of this position of observation remains semi-infinite for increasing s. Consequently the radial induction by the downstream tube remains constant, apart from the effect of varying strength and radial position of the expanding part of the vortex tube. When the effect of these variations is negligible, the result is that downstream of the disc $\partial v/\partial s < 0$ with $\partial v/\partial s > 0$ upstream of the disc, so at the disc $\partial v/\partial s = 0$. Then, by (66), the pressure at the disc is uniform and by Bernoulli's law $|\boldsymbol{v}_d| = \textit{uniform}$. This is confirmed by the isobar pattern shown in Fig. 10 and the velocity shown in Fig. 13. Apparently, the effect of the varying strength and expansion of the first part of the wake boundary does not jeopardize the line of arguments used above, for wind turbine actuator discs (in van Kuik (2018a) discs representing propellers were discussed: now the absolute velocity at the disc is not uniform).

The conclusion is that the absolute velocity at the disc is uniform, while the axial velocity is non-uniform. These results differ from the results of vortex models without wake expansion. By neglecting wake expansion, analytical treatments become into reach; see Branlard (2017) for a comprehensive treatment of this topic. These vortex models reproduce the result of momentum theory that the

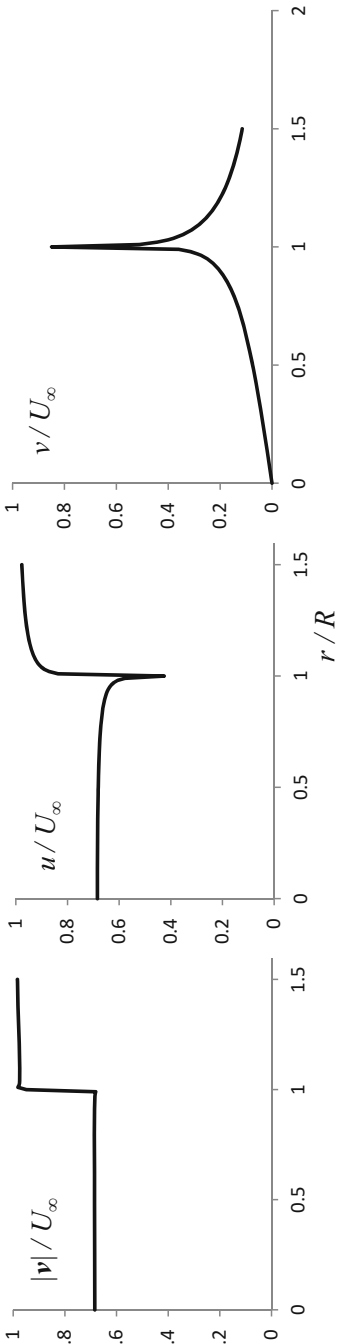

Fig. 13 The velocity components at $x = 0$ for $C_T = 8/9$

averaged induced velocity at the disc is the average of the velocities far up- and downstream. However, the present analysis reveals an essential difference between the two approaches:

- For the semi-infinite, straight vortex tube: u_d is uniform; $|\boldsymbol{v}_d|$ is non-uniform,
- For the actuator disc with wake expansion: u_d is non-uniform; $|\boldsymbol{v}_d|$ is uniform.

As long as expansion may be neglected, the vortex tube offers elegant analytical treatments providing physical insights. However, modern wind turbines operate at thrust coefficients $C_T > 0.5$ at which the expansion is significant, so the non-uniformity in u_d has to be taken into account.

The Momentum Balance Per Annulus

Applying the momentum balance to an annulus can only be done with the volume of the annulus as control volume, by which (48) becomes:

$$\Delta p A_{d,\text{ann}} - \int_{\text{ann}} \boldsymbol{e_x} \cdot \boldsymbol{e_n} p dS_{\text{ann}} = \rho \int_{A_1} u_1 (u_1 - U_\infty) dA_{1,\text{ann}}, \tag{67}$$

where S_{ann} is the surface of the annulus, $A_{d,\text{ann}}$ and $A_{1,\text{ann}}$ the cross sections of the annulus with the disc and far wake, and $\boldsymbol{e_n}$ the unit vector normal to S_{ann}. With $T_{\text{non cons}} = T_d = \Delta p A_{d,\text{ann}}$ and $T_{\text{cons}} = T_{\text{ann}} = -\int \boldsymbol{e_x} \cdot \boldsymbol{e_n} p dS_{\text{ann}}$, (61) becomes:

$$\overline{u_d} = \left(\frac{T_{\text{ann}}}{T_d} + 1 \right) \frac{U_\infty + u_1}{2}. \tag{68}$$

T_{ann} is known only after flow and pressure field calculations. In the Blade Element Momentum theory, the implicit assumption is made that $T_{\text{ann}} = 0$ by which the results of the actuator disc theory are assumed to be valid per annulus. Consequently, each annulus is considered to be independent of the other annuli. It is known that this assumption is invalid, as shown theoretically by Goorjian (1972) and numerically by Sørensen and Mikkelsen (2001), but the consequences of this assumption were assumed to be modest.

Here the ratio T_{ann}/T_d has been calculated for the annuli defined by $\Psi = \frac{n}{10}\Psi_d$ with n from 0 to 10 for flow state $C_T = 8/9$. The pressure integral is calculated with $x/R = \pm 21$ as up- and downstream limits.

Figure 14 shows the calculated distribution of u_d, the calculated average value in the respective annulus, the result of the annulus momentum theory (68) with calculated T_{ann}/T_d, and the disc averaged value $(U_\infty + u_1)/2$. The results show a very good match of the calculated average per annulus and the momentum theory value, except close to the disc edge where the steep change of u_d requires a finer resolution of annuli to capture the distribution accurately.

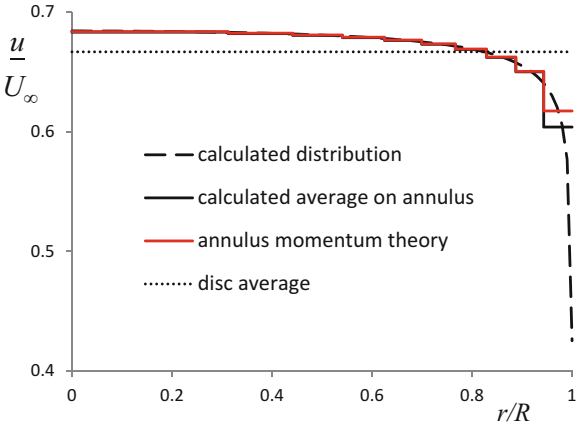

Fig. 14 u_d/U_∞ at the disc for $C_T = 8/9$: the calculated distribution, the calculated average per annulus, the result from the momentum balance per annulus, and the average. The two annuli lines coincide except in the outboard annulus

One of the remarkable results is that in the center of the disc, u is higher than $(U_\infty + u_1)/2$, so for an actuator disc, the local power coefficient exceeds the Betz-Joukowsky limit.

Sørensen and Mikkelsen (2001) have done the same analysis by viscous CFD calculations, with approximately the same result. Similar distributions of the axial velocity have been calculated by several others, e.g., Madsen (1996), Crawford (2006), Madsen et al. (2007, 2010), and Mikkelsen et al. (2009). The authors suggest several mechanisms to explain the non-uniformity of the induction, but the conclusion is that this is due to the pressure at the annuli, acting as a conservative contribution to the momentum balance.

An Engineering Model for the Velocity at the Disc

With the distribution of u_d calculated for all C_T values shown in Fig. 9, a surface fit to u_d has been made, showing the non-uniformity as defined by the ratio T_{ann}/T_d in (68). This is presented as a distribution function $G(r,\ C_T)$. Surface fitting gives the following engineering approximation:

$$\left.\begin{aligned} &G(r,\ C_T)_{0.5<C_T<1.0} = \\ &1 + a_1\left(1 - 1.00076\left(1 - \left(\frac{r}{R}\right)^{a_2}\right)^{0.0015}\right) \\ &a_1 = 62.05(1 - C_T)^{0.42} - 47.56 \\ &a_2 = 5 - 2.5(C_T - 0.8) \end{aligned}\right\} \tag{69}$$

$$G(r,\ C_T)_{0<C_T<0.5} = 1 \tag{70}$$

The surface fit matches the calculated data with a difference less than $<1\%$ for $C_T \leq 0.995$ and $r/R < 0.95$ and $<1.4\%$ for $C_T \geq 0.995$ and $r/R < 0.99$.

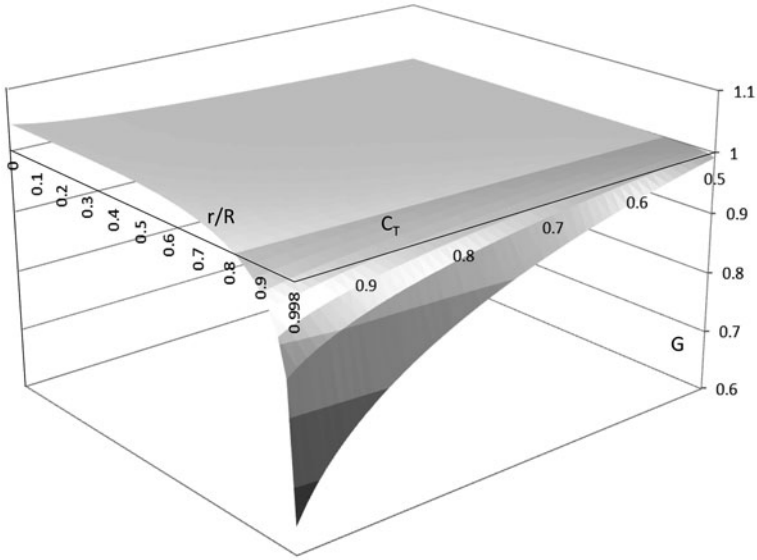

Fig. 15 The function $G(r,\ C_T)$ defined in (69) accounting for the non-uniformity of u_d

With the average velocity $\overline{u_d}$ at the disc determined by stream tube momentum theory, the distribution $u_d(r,\ C_T)$ becomes:

$$\left.\begin{aligned} \frac{u_d}{U_\infty} &= G\frac{U_\infty + u_1}{2} \\ \frac{u_1}{U_\infty} &= \sqrt{1 - C_T} \end{aligned}\right\} \tag{71}$$

with G given by (69) and (70) and shown in Fig. 15.

Analysis of Joukowsky Actuator Disc Flows

The Joukowsky distribution is described in section "Power and Thrust Expressions of Joukowsky Discs and Rotors" and shown in Fig. 5. The wake flow is characterized by a constant circulation induced by a free potential flow vortex Γ at the axis of the wake. The vortex has a core radius $\delta(x)$. The azimuthal velocity in the wake is:

$$\left.\begin{aligned} w &= \frac{\Gamma}{2\pi r} && \text{for} \quad r \geq \delta(x) \\ &= \frac{\Gamma}{2\pi\delta(x)}\mathcal{C}\left(\frac{r}{\delta(x)}\right) r && \text{for} \quad < \delta(x) \end{aligned}\right\} \tag{72}$$

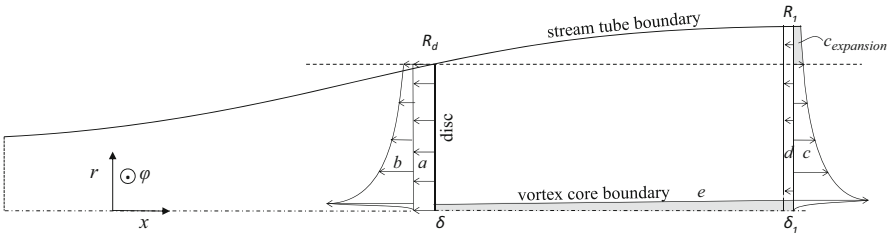

Fig. 16 Pressure distributions acting in the momentum balance sketched for an energy extracting disc flow (up) and energy adding disc (down). The arrows give the direction of the pressure fields acting on the flow. The meaning of a, b, c, d, and e is given in section "Momentum Theory for Joukowsky Discs"

The functions $\delta(x)$ and $\mathcal{C}(r/\delta(x))$ remain unspecified apart from $\mathcal{C} = 0$ for $r = 0$ and $\mathcal{C} = 1$ for $r = \delta(x)$. The core radius at the disc is indicated as $\delta = \delta(0)$ and the radius in the far wake as $\delta_1 = \delta(\infty)$. Figure 16 shows (half of) the cross section through the stream tube in the meridian plane, with the disc and fully developed wake indicated. The vortex core has an increasing radius toward the far wake due to the flow deceleration. The analysis starts with δ being non-zero after which the limit of $\delta \to 0$ is taken. The only assumption made is that:

$$\delta_1 \to 0 \quad \text{when} \quad \delta \to 0. \tag{73}$$

The Equations for a Disc with Torque and Swirl

The disc load: Equation (25) applies in the vortex core so with (72):

$$\left.\begin{aligned} \frac{1}{\rho}\Delta H &= \frac{\Omega\Gamma}{2\pi} && \text{for } r \geq \delta(x) \\ &= \frac{\Omega\Gamma}{2\pi}\frac{r}{\delta(x)}\mathcal{C}\left(\tfrac{r}{\delta(x)}\right) && \text{for } r < \delta(x) \end{aligned}\right\} \tag{74}$$

The pressure jump across the disc is given by (20) combined with (72):

$$\frac{1}{\rho}\Delta p = \frac{\Omega\Gamma}{2\pi} - \frac{1}{2}\left(\frac{\Gamma}{2\pi r}\right)^2 \quad \text{for } r \leq \delta \tag{75}$$

At the disc $\delta(0) = \delta$, so the thrust coefficient is given by (40).

The far wake outside the vortex core: For $r \geq \delta_1$ the Bernoulli equation is written as, using (74):

$$\frac{1}{\rho}(p_1 - p_\infty) = -\frac{1}{2}(u_1^2 - U_\infty^2 + w^2) + \frac{\Omega\Gamma}{2\pi}. \tag{76}$$

Differentiation with respect to r yields $\partial p_1/\partial r_1 = \rho(w^2/r_1 - u_1 \partial u_1/\partial r)$. Comparison with the expression for radial pressure equilibrium obtained from the radial component of (1) with $v = 0$:

$$\frac{\partial p_1}{\partial r_1} = \rho \frac{w^2}{r_1} \tag{77}$$

shows that u_1 is constant. By this (76) can be written as:

$$p_1 - p_\infty = -\frac{1}{2}\rho w^2 + C, \text{ with } C = constant = -\frac{1}{2}\rho(u_1^2 - U_\infty^2) + \rho\frac{\Omega\Gamma}{2\pi}. \tag{78}$$

At the wake boundary, the pressure has to be undisturbed (p_∞), so $C = \frac{1}{2}\rho w^2_{\text{wake boundary}} = \frac{1}{2}\rho(\Gamma/(2\pi R_1))^2$, with which (76) becomes:

$$p_1 - p_\infty = -\frac{1}{2}\rho w^2 + \frac{1}{2}\rho\left(\frac{\Gamma}{2\pi R_1}\right)^2. \tag{79}$$

This shows that the pressure variation in the far wake is caused only by the swirl. By substitution of (79) in (76), the second term on the right-hand side appears as a loss in H due to swirl:

$$\Delta H = \frac{1}{2}\rho(u_1^2 - U_\infty^2) + \frac{1}{2}\rho\left(\frac{\Gamma}{2\pi R_1}\right)^2. \tag{80}$$

This is consistent with the optimization of rotors according to Glauert's theory which involves minimization of the swirl; see e.g. Sørensen et al. (2015).

The vortex core: The momentum theory results are very sensitive to the choice of δ and δ_1. This is caused by the logarithmic singularity resulting from the integration of the pressure due to the azimuthal velocity: at the disc$-\rho\pi \int_R^\delta w^2 r dr = -\rho\frac{\Gamma^2}{4\pi}$ $\ln\frac{R}{\delta}$ and in the far wake $-\rho\frac{\Gamma^2}{4\pi}\ln\frac{R_1}{\delta_1}$. Several authors, e.g., de Vries (1979), Sharpe (2004), Xiros and Xiros (2007), Wood (2007), and Sørensen and van Kuik (2011b), have derived solutions of the Joukowsky momentum theory using the vortex core boundary as lower limit in the integration of velocity and pressure. This implies that the vortex core is excluded, motivated by its vanishing dimension in the limit $\delta,\ \delta_1 \to 0$. Several solutions gave the intriguing but physically infeasible result that $C_p \to \infty$ for $\lambda \to 0$. Here, in accordance with van Kuik (2017), the vortex core will be included in the momentum theory.

With $\delta(x)$ denoting the local core radius, the equivalent of the Bernoulli equation (76) in the vortex core region becomes:

$$(p_\infty - p) = \frac{\rho}{2}\left(v_s^2 - U_\infty^2 + \left(\frac{\Gamma}{2\pi\delta(x)}\mathcal{C}\left(\frac{r}{\delta(x)}\right)\right)^2\right) - \frac{\Omega\Gamma}{2\pi}\frac{r}{\delta(x)}\mathcal{C}\left(\frac{r}{\delta(x)}\right), \tag{81}$$

where $v_s = \sqrt{u^2 + v^2}$ is the velocity in the meridian plane. The terms v_s, U_∞ and the last term on the right-hand side remain finite when $\delta(x) \to 0$. The remaining contribution becomes infinite in this limit, so dominates the pressure:

$$\lim_{\delta(x)\to 0}\frac{1}{\rho}(p_\infty - p) = \frac{1}{2}\left(\frac{\Gamma}{2\pi\delta(x)}\mathcal{C}\left(\frac{r}{\delta(x)}\right)\right)^2. \tag{82}$$

Now the vortex core itself is taken as control volume for the axial momentum balance. Given the assumption of inviscid, isentropic Euler flow, the vortex core boundary is a stream surface, where $\mathcal{C} = 1$. With v_s remaining finite, the momentum flux through the control volume boundary becomes 0 for $\delta(x) \to 0$, so the momentum balance reduces to a balance of pressures acting on the control volume boundary, integrated as a load in x direction:

$$\int_0^\delta (p - p_\infty)2\pi r dr - \int_0^{\delta_1}(p_1 - p_\infty)2\pi r dr + \int_\delta^{\delta_1}(p(x,\delta(x)) - p_\infty)2\pi\delta(x)d\delta(x) = 0, \tag{83}$$

where the path of integration of the third integral is the core boundary $\delta(x)$ with $0 \le x \le x_1$. The third integral is evaluated with (82), so:

$$\begin{aligned}\lim_{\delta(x)\to 0}\left[\int_\delta^{\delta_1}(p(x,\delta(x)) - p_\infty)2\pi\delta(x)d\delta(x)\right] &= -\frac{1}{2}\rho\int_\delta^{\delta_1}\frac{\Gamma^2}{2\pi\delta(x)}d\delta(x)\\ &= -\rho\frac{\Gamma^2}{4\pi}\ln\frac{\delta_1}{\delta}.\end{aligned} \tag{84}$$

The combination of (83) and (84) gives:

$$\lim_{\delta(x)\to 0}\left[\int_0^\delta (p - p_\infty)2\pi r dr - \int_0^{\delta_1}(p_1 - p_\infty)2\pi r dr\right] = \rho\frac{\Gamma^2}{4\pi}\ln\frac{\delta_1}{\delta}, \tag{85}$$

irrespective of the choice of core model δ, $\mathcal{C}$. This result will be used in section "Momentum Theory for Joukowsky Discs" where the momentum balance for the entire stream tube is studied.

Momentum Theory for Joukowsky Discs

The momentum balance (48) with the stream tube as control volume (see Fig. 16) is written as:

$$T - \int_{A_1} (p_1 - p_\infty) 2\pi r dr = \rho \int_{A_1} u_1 (u_1 - U_\infty) dA_1. \tag{86}$$

The boundaries of the momentum balance volume are the stream tube boundary and the cross sections A_∞ and A_1 far up- and downstream. The pressure at the stream tube boundary does not contribute to the momentum balance (see section "The Momentum Balance") so is not included in (86).

Figure 16 shows the pressure distributions appearing on the left-hand side of (86) including the thrust:

- a constant pressure jump across the disc giving the jump in Bernoulli parameter H, according to the first term on the right-hand side of (75).
- b pressure distribution due to jump in w for $r \geq \delta$ according to the second term on the right-hand side of (75). This term conserves H.
- c apart from correction by (d), the pressure distribution in the far wake due to the w distribution is identical to (b) for $r \geq \delta_1$, according to the first term at the right-hand side of (79), conserving H.
- d a correction to (c) to achieve $p_1 - p_\infty = 0$, according to the second term on the right-hand side of (79).
- e the contribution by the vortex core cross sections, (85).

When all contributions are expressed in Γ by (72) and (74), integrated, subjected to $\lim \delta \to 0$, substituted in (86), and divided by the disc surface πR^2, the result is:

$$\overset{a}{\frac{\Omega\Gamma}{2\pi}} - \overset{d}{\frac{1}{2}\left(\frac{\Gamma}{2\pi R}\right)^2} - \left(\frac{\Gamma}{2\pi R}\right)^2 \left[\overset{b}{\ln\frac{R}{\delta}} - \overset{c}{\ln\frac{R_1}{\delta_1}} - \overset{e}{\ln\frac{\delta_1}{\delta}}\right] = u_1(u_1 - U_\infty)\left(\frac{R_1}{R}\right)^2 \tag{87}$$

where the terms on the left-hand side have been named (a) to (e) in accordance with Fig. 16. The logarithmic terms reduce to $\ln(R/R_1)$, so only the wake expansion area ($c_{\text{expansion}}$) contributes to this term. This contribution is shown as a gray area in Fig. 16. The mass balance is:

$$\frac{\overline{u_d}}{u_1} = \left(\frac{R_1}{R}\right)^2 \tag{88}$$

with the bar above u_d indicating that it is the average value. The energy balance follows from (80):

$$\frac{\Omega\Gamma}{2\pi} - \frac{1}{2}\left(\frac{\Gamma}{2\pi R_1}\right)^2 = \frac{1}{2}(u_1^2 - U_\infty^2). \tag{89}$$

Mixing (87) and (88) simplifies the momentum balance, yielding:

$$\frac{\Omega\Gamma}{2\pi} - \frac{1}{2}\left(\frac{\Gamma}{2\pi R}\right)^2 - \left(\frac{\Gamma}{2\pi R}\right)^2 \ln\frac{R}{R_1} = \overline{u_d}(u_1 - U_\infty). \tag{90}$$

As in section "Power and Thrust Expressions of Joukowsky Discs and Rotors" the non-dimensional vortex $q = \Gamma/(2\pi R U_\infty)$ is introduced. Herewith (74) becomes:

$$\frac{1}{\rho}\frac{\Delta H_d}{U_\infty^2} = \lambda q, \tag{91}$$

and the momentum balance:

$$-2\lambda q + q^2\left(1 + \ln\left(\frac{R}{R_1}\right)^2\right) = 2\frac{\overline{u_d}}{U_\infty}\left(1 - \frac{u_1}{U_\infty}\right), \tag{92}$$

as well as the energy balance:

$$-2\lambda q + q^2\left(\frac{R}{R_1}\right)^2 = \left(1 - \left(\frac{u_1}{U_\infty}\right)^2\right). \tag{93}$$

By mixing (92) and (93), the velocity at the disc can be written as:

$$\frac{\overline{u_d}}{U_\infty} = \frac{1}{2}\left(\frac{u_1}{U_\infty} + 1\right)\frac{2\lambda q - q^2\left(1 + \ln\left(\frac{R}{R_1}\right)^2\right)}{2\lambda q - q^2\left(\frac{R}{R_1}\right)^2}. \tag{94}$$

This equation is equivalent to (61), indicating that the ratio contains conservative and non-conservative contributions. This will be discussed in section "The Role of Swirl".

An analytical solution of (92) and (93) is not found. An implicit expression of u_1/U_∞ in the independent variables λ, q is obtained by writing (93) as an expression for u_1 with the help of (88) and substituting this in (92):

$$\frac{\left(1 - \frac{u_1}{U_\infty}\right)\frac{u_1}{U_\infty}q^2}{1 - 2\lambda q - \left(\frac{u_1}{U_\infty}\right)^2} = \left(-q\lambda - \frac{1}{2}q^2\left(1 - \ln\left(\frac{q^2}{1 - 2\lambda q - (\frac{u_1}{U_\infty})^2}\right)\right)\right). \tag{95}$$

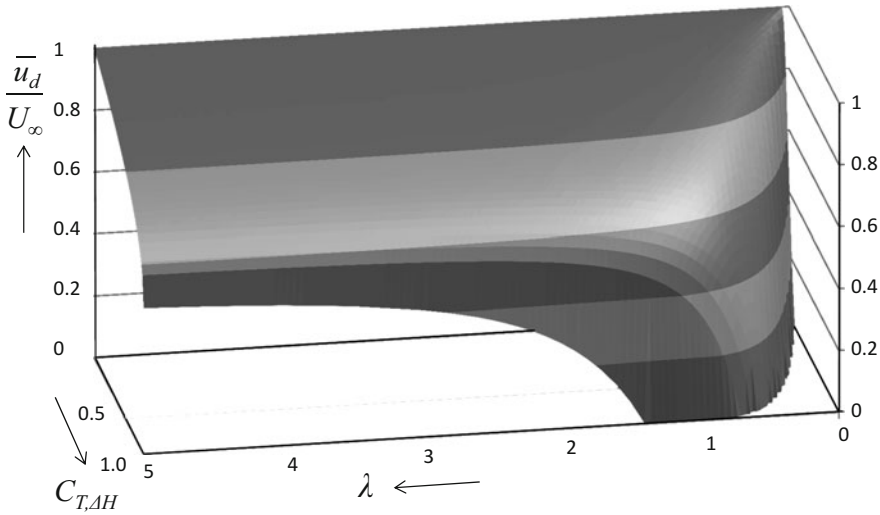

Fig. 17 The axial velocity $\overline{u}_d$ at the disc for $0 \leq C_{T,\Delta H} \leq 1$, $0 \leq \lambda \leq 5$

This can be solved numerically for u_1/U_∞. The wake expansion or contraction follows by (93) and the velocity at the disc by (92). The power coefficient is given by (37) and the thrust coefficient by (40).

Figures 17 and 18 show the solutions of (95) and (37) for $0 \leq \lambda \leq 5$ and $0 < C_{T,\Delta H} \leq 1$. Several particularities can be observed, to be addressed in the next sections:

- A minimum λ exists at which the velocity at the disc is 0. For a given $C_{T,\Delta H}$, a lower λ is not possible.
- The maximum efficiency C_p of energy extracting discs decreases to 0 for decreasing λ.

Limit Values: $\lambda \to \infty, \lambda \to 0$, $C_{p,\max}$

Results for $\lambda \to \infty$, $\lambda \to 0$ *:* For large values of λ, the angular momentum should go to 0, and the momentum theory should become the one-dimensional theory, recovering the well-known Betz-Joukowsky maximum value for C_p. According to (91) q is inversely proportional to λ for constant ΔH. In the balances (92) and (93), the q^2 terms vanish for $\lambda \to \infty$, so ΔH becomes Δp with which the Froude momentum theory equations (50) and (51) are indeed recovered.

For the limit $\lambda \to 0$, the energy balance (93) shows that the highest value for $q^2(R/R_1)^2$ is obtained for $u_1/U_\infty = 0$:

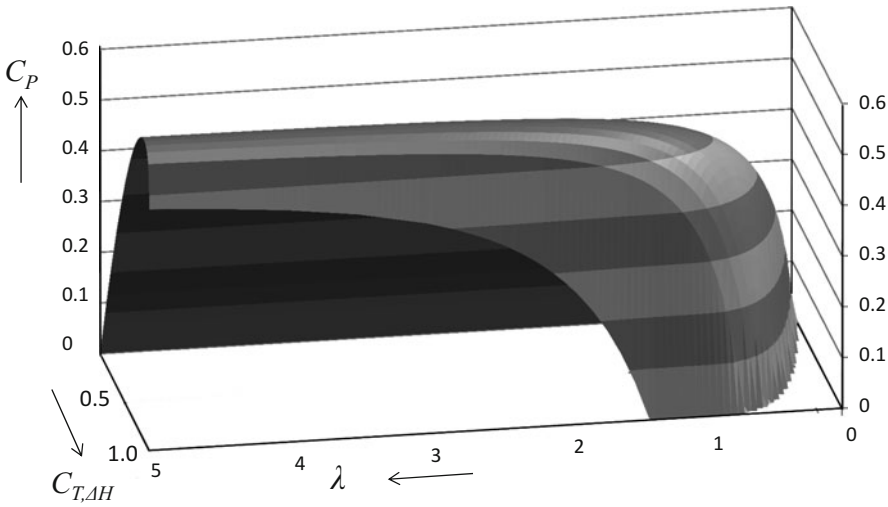

Fig. 18 The power coefficient C_p for $0 \le C_{T,\Delta H} \le 1$, $0 \le \lambda \le 5$

$$-2\lambda q + q^2 \left(\frac{R}{R_1}\right)^2 = 1. \tag{96}$$

With $u_1/U_\infty = 0$ the right-hand side of the momentum balance is 0 as is clear from (87), by which it becomes:

$$-2\lambda q + q^2 \left(1 - \ln\left(\frac{R_1}{R}\right)^2\right) = 0. \tag{97}$$

Elimination of q^2 from (96) and (97) gives the wake expansion for the highest q, lowest λ with $u_1 = 0$:

$$\left(\frac{R_1}{R}\right)^2 \left(1 - \ln\left(\frac{R_1}{R}\right)^2\right) = \frac{2\lambda q}{2\lambda q + 1}. \tag{98}$$

As an example, $2\lambda q = \Delta H/(\frac{1}{2}\rho U_\infty^2) = -8/9$ results in $R_1/R = 2.77$, $q = -0.924$ from (96) and $\lambda = 0.48$. Both $\overline{u_d}$ and u_1 are 0, but the ratio of $\overline{u_d}/u_1 \to 7.69$. This flow state is characterized by a full blockage by the disc, creating a wake with azimuthal flow only, so there is no change in axial momentum. A lower value of λ is not possible for this value of λq. For $\lambda q = 0$ with $\lambda = 0$, (98) gives $\ln(R_1/R)^2 = 1$ or $R/R_1 = \sqrt{e}$, with which (96) gives $R_1/R = -q = \sqrt{e} = 1.648$ although $\overline{u_d} = u_1 = 0$. In the wake only the azimuthal velocity is non-zero, reaching $qR/R_1 = -1$ at the far wake boundary $r = R_1$. The wake expansion is close to the experimental value ≈ 1.6 of the wake expansion behind a solid disc reported in Craze (1977).

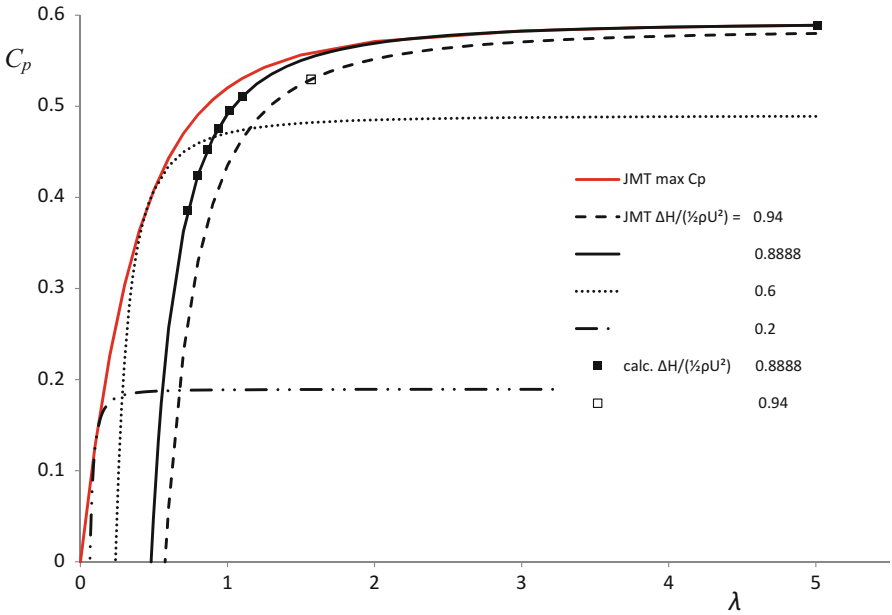

Fig. 19 The Joukowsky momentum theory results (black lines), calculated values (τ, see section "Numerical Results"), and the maximum wind turbine C_p (red line)

The maximum efficiency: Figure 19 shows the maximal attainable C_p and the $C_p - \lambda$ curves for some values of $C_{T,\Delta H}$. For $\lambda \to 0$ the efficiency $C_p \to 0$, and for $\lambda \to \infty$ C_p increases to the Betz-Joukowsky maximum 16/27. The $C_{p,\max} - \lambda$ curve resembles the performance curve of discs with the Betz-Goldstein distribution of circulation as published by Okulov (2014) and Wood (2015). These performance curves have been compared in van Kuik (2017), showing that the Joukowsky distribution gives a slightly higher C_p than the Betz-Goldstein-based distributions, with the difference vanishing for higher λ. Okulov and Sørensen (2010) have compared rotors having a Joukowsky- and Betz-Goldstein-based distribution. The same conclusion is drawn: Joukowsky rotors perform slightly better than Betz-Goldstein-based rotors.

Numerical Results

The numerical model: The numerical method described in section "Numerical Assessment of Actuator Disc Performance" has been adapted to include wakes with swirl by defining the force free condition for the wake boundary. Equivalent to (76), with p_1 replaced by p and u_1 by $v_s = \sqrt{u^2 + v^2}$, this gives:

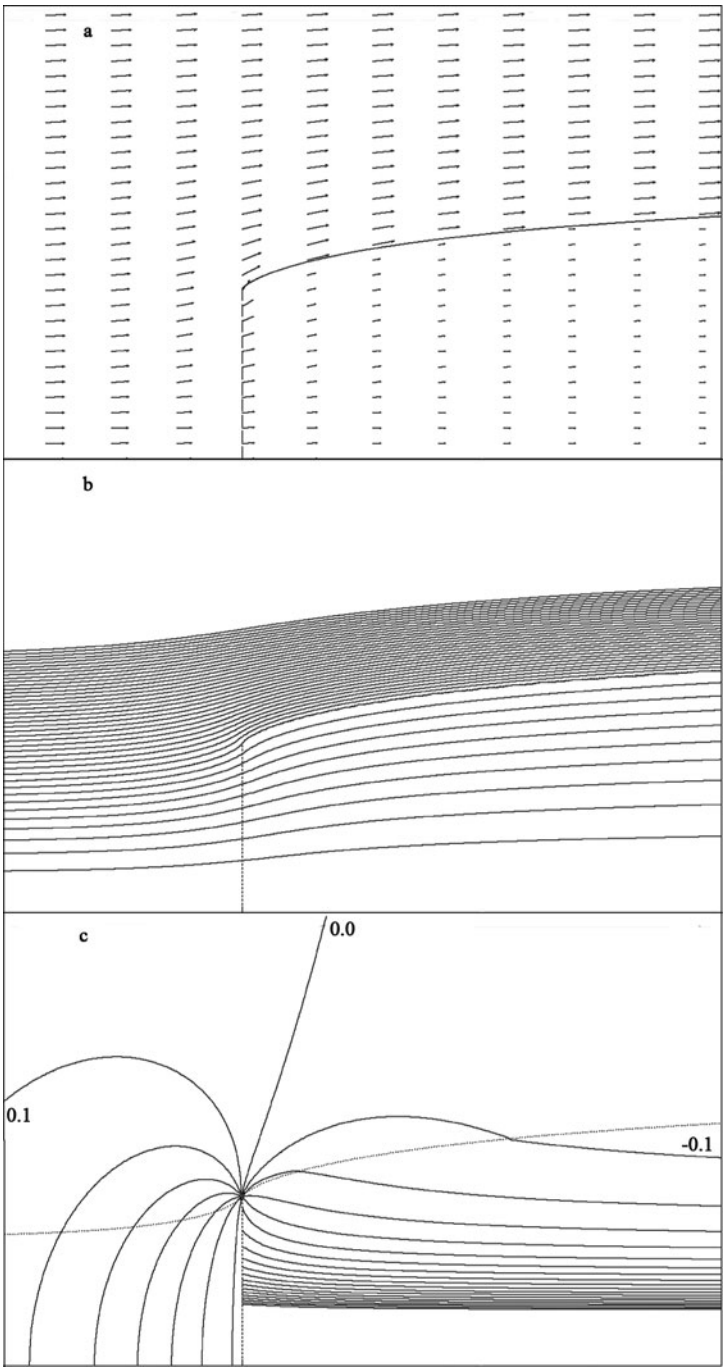

Fig. 20 for $C_T = 8/9,\ \lambda = 1$: (**a**) shows the velocity field and wake boundary, (**b**) stream tube value Ψ/Ψ_1, (**c**) isobars $(p - p_\infty)/|\Delta p|$, both with increments of 0.1. Isobars close to the wake axis are not plotted

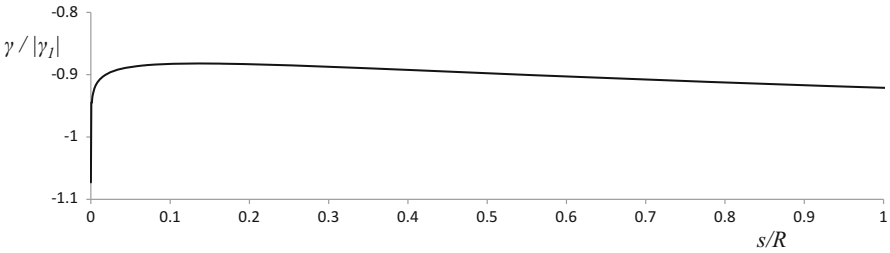

Fig. 21 The distribution of the vortex sheet strength $\gamma(s)$ as a function of the distance s/R measured along the sheet, for $C_T = 8/9$, $\lambda = 1$

$$\Delta_{\text{wake boundary}} \left(\frac{1}{2} \left(v_s^2 + w^2 \right) \right) = \frac{\Omega \Gamma}{2\pi} \tag{99}$$

Figure 19 shows the calculated $C_p(\lambda)$ for fixed values of $2\lambda q = \Delta H / \frac{1}{2} \rho U_\infty^2$ and the momentum theory values. The data match very well. For $\lambda = 5$ the difference in C_p compared with the values for $\lambda \to \infty$, so with the one-dimensional momentum theory, is less than 0.7%. Consequently, swirl may be ignored for $\lambda > 5$.

Flow details at $\lambda = 1$ *compared with* $\lambda = \infty$:

Figure 20 shows the streamlines and isobars of the disc flow with $\lambda = 1$ for $C_{T,\Delta H} = 8/9$. The isobars in the wake show the pressure gradient due to the swirl. The distribution of the vortex sheet strength γ is shown in Fig. 21, and the absolute, axial, and radial velocity at the upstream side of the disc in Fig. 22. The figures can be compared with the equivalent Figs. 10, 11, and 13 for the Froude disc flow, so for infinite λ.

The velocity at the disc: Figure 22 shows the velocity components at the upstream side of the disc for $\lambda = 1$, with constant $|\boldsymbol{v}|$ (with a deviation of 2%).

For all load cases with $\lambda > 5$, the same is found: the absolute velocity in the meridian plane, $\sqrt{u^2 + v^2}$, is constant, irrespective of $C_{T,\Delta H}$ or λ, (with a maximum deviation of 1%).

In section "The Velocity Distribution at the Disc" an explanation is given for the absolute velocity at the Froude disc to be uniform. The same explanation holds for the constant meridian velocity at the Joukowsky disc, as the azimuthal component w has no impact at the line of arguments in section "The Velocity Distribution at the Disc".

The Momentum Balance Per Annulus of Joukowksy Disc Flows

The balance for the stream tube is defined by (86). In this equation the pressure acting at the stream tube boundary is absent as discussed in section "The Momentum Balance". When applying the momentum balance to an annulus instead of the entire

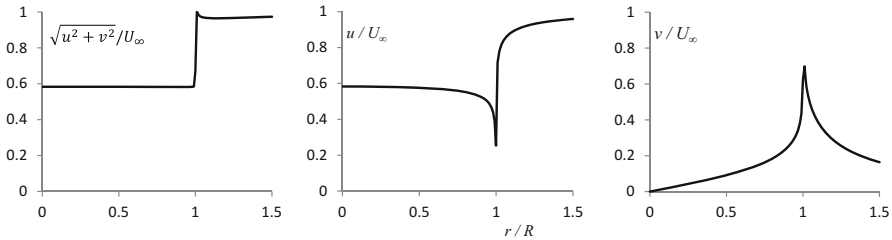

Fig. 22 The velocity components at the upstream side of the disc for $C_{T,\Delta H} = 8/9$, $\lambda = 1$

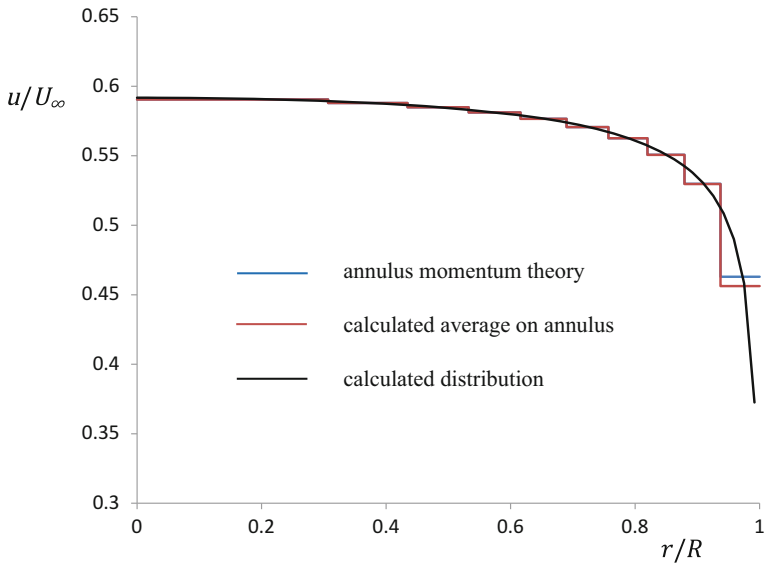

Fig. 23 u/U_∞ at the disc for $C_{T,\Delta H} = 8/9$ and $\lambda = 1$: the calculated distribution, the calculated average per annulus and the result from the momentum balance per annulus. The two annuli lines coincide except in the outboard annulus

stream tube, the same procedure is applied as in section "The Momentum Balance Per Annulus". Figure 23 shows the distribution of u_d resulting from the flow field calculation, the associated average value per annulus, and the value resulting from (68). As in Fig. 14, the calculated average per annulus coincides everywhere except at the disc edge with the momentum theory value. This confirms the results from the Froude discs in section "Analysis of Froude Actuator Disc Flows": the annuli cannot be assumed as independent, as the pressure field contributes to the axial momentum exchange leading to the non-uniform distribution of u_d.

The Role of Swirl

The ratio in (94) is the ratio between the left-hand sides of the momentum balance (92) and energy balance (93) or, in other words, between the total load exerted on the flow in the stream tube control volume and the non-conservative load which is the load performing work. By this, (94) is equivalent to (61) which shows how conservative forces affect the momentum balance: the induced velocity at the disc deviates from Froude's result. Inspection of the pressure distributions contributing to the momentum balance as shown in Fig. 16 and listed in section "Momentum Theory for Joukowsky Discs" shows that:

- all distributions appear in the momentum balance (87) or (92) with (b), (c), and (e) cancelling each other apart from $(c_{\text{expansion}})$
- distributions (a) and (d) appear in the energy balance (89) or (93), so are non-conservative
- distributions (b), (c), and (e) do not appear in the energy balance, so are conservative.

Evaluation of $(a + d + c_{\text{expansion}})$ for the counter of the ratio $T_{\text{total}}/T_{\text{cons}}$ in (61) and $(a + d)$ for the denominator returns (94). The difference between the momentum theory results for Froude and Joukowsky discs is caused by the swirl-related pressure in the far wake: the conservative $(c_{\text{expansion}})$ and the non-conservative (d).

The swirl-related pressure distributions (b) and (c) are conservative as the gradient of the pressure and azimuthal velocity results in a conservation of potential and kinetic energy: $\partial(\Delta p_w + \frac{1}{2}\rho w^2/\partial r = 0$, as discussed right after (26). Still swirl has an impact on the energy balance by distribution (d). The change of H from undisturbed to its value in the far wake is given by (80) with the first term at the right-hand side expressing the change in kinetic energy and the second term, being the pressure (d), the change in potential energy.

On the Use of Actuator Disc Theory in BEM

Blade and Tip Effects

BEM uses the Froude or Joukowsky actuator disc momentum theory per annulus without taking the pressure at the boundary of the annuli into account, unlike the balance in section "The Momentum Balance Per Annulus". In case of straightforward optimization of a rotor in straight, uniform flow, all annuli will give the same result leading to a radially uniform u_d. Furthermore, the resulting velocity is also azimuthally uniform as the momentum theory treats the rotor as a disc. To remove these deficiencies, BEM is always used with corrections or engineering additions to the momentum balance. The most important correction to the momentum balance in uniform flow is the correction for the finite number of blades, usually the one of Prandtl-Glauert. Prandtl has derived it as a correction for a finite number of blades

to the disc model of Betz (1919), in an appendix to Betz's paper. The model of Betz is briefly described in section "The Actuator Disc". Glauert (1935, ch. VII-4) has adapted Prandtl's correction as to apply it at the blade position instead of the azimuthally averaged disc. Neither Prandtl nor Glauert has called the correction a tip correction, although this is the commonly used name instead of "number of blade correction." The reason is that the correction, in which the number of blades is a major parameter, modifies the induction near the blade tip and, by doing so, also the blade loading.

The two most important limitations of the actuator disc theory, being the treatment of a rotor as a disc and the inability to provide a radial distribution of the velocity, are eliminated by the Prandt-Glauert correction. This is a remarkable achievement, as the present application is far away from the origin of the correction: Prandtl derived it as a 2-D correction for the 3-D optimal Betz circulation distribution for lightly loaded discs, but it is applied to BEM which optimizes for a heavily loaded Joukowsky distribution.

After Glauert the correction has been modified by many, as can be read in Sørensen et al. (2015, chapter 8) and Branlard (2017, chapter 13), by fine-tuning and validating it with experiments and CFD calculations. The modification by Shen et al. (2005, 2014) to account for the geometry of the blade tip will be used in the next section.

Comparison of Actuator Disc and BEM Induction

At the time Prandtl published his correction, the velocity distribution at the Froude disc was not yet known. In section "Analysis of Froude Actuator Disc Flows" this distribution has been calculated for a range of thrust coefficients, so it is worthwhile to compare this distribution with the results of annulus-based momentum theory with the Prandtl-Glauert-Shen (PGS) tip correction as used in BEM.

The PGS correction is used in the momentum balance to solve a_B:

$$C_t F_1 = 4 a_B F (1 - a_B F), \tag{100}$$

where F is the Prandtl-Glauert correction and F_1 the Shen correction:

$$F = \frac{2}{\pi} \cos^{-1} \left[\exp \left(-\frac{B}{2} \left(\frac{R}{r} - 1 \right) \frac{1}{\sin(\theta)} \right) \right], \tag{101}$$

where θ is the local inflow angle, with $\sin(\theta) = u_B / \sqrt{(\Omega r - w_B)^2 + u_B^2}$ and with subscript B indicating the velocity at the blade position, and:

$$\left.\begin{aligned} F_1 &= \frac{2}{\pi}\cos^{-1}\left[\exp\left(-g\frac{B}{2}\left(\frac{R}{r}-1\right)^n\frac{1}{\sin(\theta)}\right)\right] \\ g &= \exp\left[\frac{0.125(B\lambda-21)}{1-2k}\right]+0.1 \\ n &= 1+0.5k \end{aligned}\right\} \tag{102}$$

where k is the minimum value of chord-to-radius derivative at the tip. The value $k = -0.45$, used by Shen, is used here unmodified. When B, λ are given, F and F_1 are known except for u_B or the induction $a_B = (1 - u_B/U_\infty)$. In BEM C_t depends on u_B and on local aerofoil characteristics, so (100) has to be solved iteratively. For a given $C_t F_1$, the quantity $a_B F$ is solved as the azimuthally averaged induction resulting from the momentum theory without any radial dependency of the results. The local induction a_B follows after division by F, after which C_t can be renewed until convergence is reached.

For the actuator disc, C_t is predefined, given by (47). Here we use C_t without the q^2 term, as discussed in section "Power and Thrust Expressions of Joukowsky Discs and Rotors". The momentum theory solution of (100) obtained with this C_t will be compared with the calculated actuator disc results obtained in section "Analysis of Froude Actuator Disc Flows", for the same C_t. The radial distribution of the axial velocity is given by the function G, described by (69) and (70) and shown in Fig. 15. It is used in combination with the local momentum equation:

$$\left.\begin{aligned} C_t &= 4a(1-a) \\ 1-a_B &= G(1-a) \end{aligned}\right\} \tag{103}$$

The first equation gives the induction a as if the local and disc-averaged momentum equations are the same, the second equation gives the local value.

In van Kuik et al. (2015a) the comparison of both methods, (100) and (103), is done for the load cases representing an optimal rotor with $C_T = 8/9$, $\lambda = 7$, a heavily loaded rotor with $C_T = 0.97$, $\lambda = 7$, and a very fast running rotor with $C_T = 8/9$, $\lambda = 20$. For all rotors $B = 3$. The results are shown in Fig. 24, presenting u_B as resulting from the PGS correction and G function. The PGS correction has little effect for $r < 0.8R$, so the axial velocity is lower than the G function for $r/R < 0.8$. For $r/R > 0.8$ the actuator disc line G corresponds reasonably well with the PGS corrected results.

The reasonable correspondence between the induction function G and the PGS corrected induction is confirmed by a similar correspondence between the induction function G and the induction at the blade position of a three-bladed rotor, calculated by a lifting line and actuator line method; see van Kuik et al. (2015a). Given this, one might consider to use the G function in BEM instead of the PGS correction. However only a few loadcases in straight uniform flow have been examined for one specific (constant) blade circulation. Much more load cases and off-design conditions have to be tested to fine-tune and validate the G function.

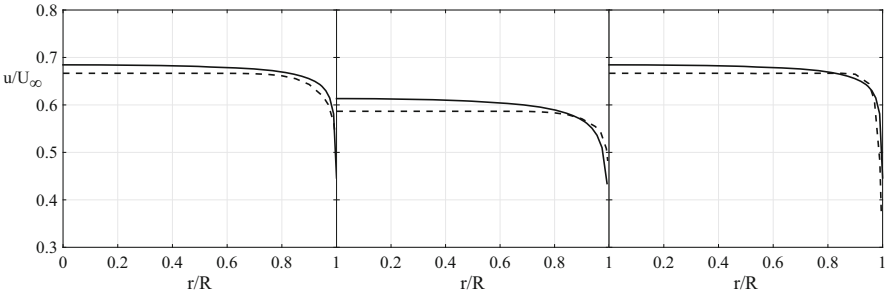

Fig. 24 The axial velocity distribution obtained from the momentum theory + PGS correction (dash line) and actuator disc function G (solid line). Left $C_T = 8/9$, $\lambda = 7$, middle $C_T = 0.97$, $\lambda = 7$, right $C_T = 8/9$, $\lambda = 20$

Cross-References

▶ History of Aerodynamic Modelling
▶ Pragmatic Models: BEM with Engineering Add-Ons
▶ Rotor Blade Design, Number of Blades, Performance Characteristics

References

Anderson HB, Milborrow DJ, Ross JN (1982) Performance and wake measurements on a 3 m diameter horizontal axis wind turbine rotor. In: Proceedings of 4th international symposium on wind energy systems. Stockholm, BHRA (1982)

Batchelor GK (1970) An introduction to fluid dynamics. Cambridge University Press, Cambridge. https://doi.org/10.1017/CBO9805II800955

Betz A (1919) Schraubenpropeller mit geringstem Energieverlust. Reprint of 4 famous papers by Universitatsverlag Gottingen

Betz A (1920) Das Maximum der theoretisch möglichen Ausnützung des Windes durch Windmotoren. Zeitschrift für das gesamte Turbinenwesen 26:307–309

Branlard E (2017) Wind turbine aerodynamics and vorticity-based methods. Springer International Publishing. ISBN 9783319551630. https://doi.org/10.1007/978-3-319-55164-7

Burton T, Jenkins N, Sharpe DJ, Bossanyi E (2011) Wind energy handbook. Wiley. ISBN 9780471489979. https://doi.org/10.1002/0470846062

Crawford C (2006) Re-examination of the precepts of the blade element momentum theory for coning rotors. Wind Energy 9:457–478. https://doi.org/10.1002/we/197

Craze DJ (1977) On the near wake behind a circular disc. In: 6th Australasian hydraulics and fluid mechanics conference, pp 282–286

de Vries O (1979) Fluid dynamic aspects of wind energy conversion, AGARD-AG-243. AGARD, Amsterdam. ISBN 9283513266, 9789283513261

Froude RE (1889) On the part played in propulsion by differences of fluid pressure. In: 13th session of the institution of naval architects, vol 30, pp 390–405

Glauert H (1926) The analysis of experimental results in the windmill brake and vortex ring state of an airscrew. Aeronautical Research Council R&M 1026, London

Glauert H (1935) The general momentum theory. In: Aerodynamic theory volume IV division L. Springer, Berlin, reprinted as Dover Edition

Goldstein S (1929) On the vortex theory of screw propellers. Proc R Soc Lond A 123:440–465

Goorjian PM (1972) An invalid equation in the general momentum theory of the actuator disk. AIAA J 10(4):543–544

Haans W, Sant T, Van Kuik GAM, van Bussel GJW (2008) HAWT near-wake aerodynamics, Part I: axial flow conditions. Wind Energy 11:245–264. https://doi.org/10.1002/we.262

Hansen MOL (2008) Aerodynamics of wind turbines. Earthscan. ISBN 9781844074389

Joukowsky JN (1912) Vortex theory of the screw Propeller I. Trudy Avia Raschetno-Ispytatelnogo Byuro (in Russian) Also published in Gauthier-Villars et Cie.(eds) Theéorie Tourbillonnaire de l'Hélice Propulsive, Quatrième Mémoire. 1929; 1:1–47, 16(1):1–31

Joukowsky JN (1918) Vortex theory of the screw propeller IV. Trudy Avia Raschetno-Ispytatelnogo Byuro (in Russian] Also published in Gauthier-Villars et Cie.(eds Théorie Tourbillonnaire de l'Hélice Propulsive, Quatrième Mémoire. 1929; 4:123–198, 3:1–97

Joukowsky JN (1920) Joukowsky windmills of the NEJ type. In: Transactions of the central institute for aero-hydrodynamics of Moscow, pp 405–430

Lignarolo LEM, Ferreira CS, van Bussel GJW (2016a) Experimental comparison of a wind turbine and of an actuator disc wake. J Renew Sustain Energy 8(023301):1–26. ISSN 1941-7012. https://doi.org/10.1063/1.4941926

Lignarolo LEM, Mehta D, Stevens RJAM, Yilmaz AE, Meyers J, Andersen SJ, van Kuik GAM, Meneveau C, Holierhoek J, Simão Ferreira CJ, Ragni D, van Bussel GJW (2016b) Validation of four LES and a vortex model against PIV measurements of the near wake of an actuator disk and a wind turbine. Renew Energy 94:510–523. ISSN 09601481. https://doi.org/10.1016/j.renene.2016.03.070

Madsen HA (1996) A CFD analysis of the actuator disc flow compared with momentum theory results. In: 10th IEA aerodynamic expert meeting, pp 109–124

Madsen HA, Mikkelsen RF, Øye S, Bak C, Johansen J (2007) A detailed investigation of the blade element momentum (BEM) model based on analytical and numerical results and proposal for modifications of the BEM model. J Phys Conf Ser 75:012016. ISSN 1742-6596. https://doi.org/10.1088/1742-6596/75/1/012016

Madsen HA, Bak C, Døssing M, Mikkelsen RF, Øye S (2010) Validation and modification of the blade element momentum theory based on comparisons with actuator disc simulations. Wind Energy 13:373–389. https://doi.org/10.1002/we359

Martínez-Tossas LA, Churchfield MJ, Meneveau C (2017) Optimal smoothing length scale for actuator line models of wind turbine blades based on Gaussian body force distribution. Wind Energy 20(6):1083–1106. https://doi.org/10.1002/we.2081

Medici D, Alfredsson PH (2006) Measurements on a wind turbine wake: 3D effects and bluff body vortex shedding. Wind Energy 9:219–236. https://doi.org/10.1002/we/156

Mikkelsen RF, Øye S, Sørensen JN, Madsen HA, Shen WZ (2009) Analysis of wake expansion and induction near tip. In: Proceedings EWEC2009, Marseille

Okulov VL (2014) Limit cases for rotor theories with Betz optimization. J Phys Conf Ser 524:012129. ISSN 1742-6596. https://doi.org/10.1088/1742-6596/524/1/012129

Okulov VL, Sørensen JN (2010) Maximum efficiency of wind turbine rotors using Joukowsky and Betz approaches. J Fluid Mech 649:497–508. ISSN 0022-2120. https://doi.org/10.1017/S0022112010000509

Okulov VL, van Kuik GAM (2012) The Betz – Joukowsky limit: on the contribution to rotor aerodynamics by the British, German and Russian scientific schools. Wind Energy 15:335–344. https://doi.org/10.1002/we/464

Okulov VL, Sørensen JN, Wood DH (2015) Rotor theories by Professor Joukowsky: vortex theories. Prog Aerosp Sci 73:19–46. ISSN 03760421. https://doi.org/10.1016/j.paerosci.2014.10.002

Øye S (1990) A simple vortex model. In: McAnulty KF (ed) Third IEA symposium on the aerodynamics of wind turbine, pp 1–15, Harwell. ETSU

Parra EA, Boorsma K, Schepers JG, Snel H (2016) Momentum considerations on the New MEXICO experiment. J Phys Conf Ser 753:072001. ISSN 1742-6588. https://doi.org/10.1088/1742-6596/753/7/072001

Prandtl L (1918) Tragflügeltheorie I. Mitteilung. Nachrichten der Königlichem Gesellschaft der Wissenschaften zü Göttingen, Mathematisch-physikalische Klasse, pp 451–477

Saffman PG (1992) Vortex dynamics, monographs edition. University Press, Cambridge. ISBN 052142058X, 9780521420587

Sharpe DJ (2004) A general momentum theory applied to an energy-extracting actuator disc. Wind Energy 7(3):177–188. ISSN 1095-4244. https://doi.org/10.1002/we.118

Shen WZ, Mikkelsen RF, Sørensen JN, Bak C (2005) Tip loss corrections for wind turbine computations. Wind Energy 8(4):457–475. ISSN 1095-4244. https://doi.org/10.1002/we.153

Shen WZ, Zhu WJ, Sørensen JN (2014) Study of tip loss corrections using CFD rotor computations. J Phys Conf Ser 555:012094. ISSN 1742-6588. https://doi.org/10.1088/1742-6596/555/1/012094

Sørensen JN (2015) General momentum theory for horizontal axis wind turbines. Springer International Publishing, Heidelberg. ISBN 978-3-319-22113-7. https://doi.org/10.1007/978-3-319-22114-4

Sørensen JN, Mikkelsen RF (2001) On the validity of the blade element momentum method. In: EWEC2001, Copenhagen, pp 362–366

Sørensen JN, van Kuik GAM (2011a) Aerodynamic aspects of wind energy conversion. Annu Rev Fluid Mech 43(1):427–448. ISSN 0066-4189. https://doi.org/10.1146/annurev-fluid-l22l09-l6080l

Sørensen JN, van Kuik GAM (2011b) General momentum theory for wind turbines at low tip speed ratios. Wind Energy 14:821–839. https://doi.org/10.1002/we.423

Sørensen JN, Shen WZ, Munduate X (1998) Analysis of wake states by a full field actuator disc model. Wind Energy 88:73–88. https://doi.org/10.1002/(SICI)1099--1824(199812)1:2<73::AID--WEI2>3.0.CO;2-L

Sørensen JN, Dag KO, Ramos-García N (2014) A new tip correction based on the decambering approach. J Phys Conf Ser 524(Torque2014):012097. ISSN 1742-6596. https://doi.org/10.1088/1742-6596/524/1/012097

Sørensen JN, Dag KO, Ramos-García N (2015) A refined tip correction based on decambering. Wind Energy 19(5):787–802. https://doi.org/10.1002/we/1865

Thoma D (1925) Grundsatzliches zur einfachen Strahltheorie der Schraube. Zeitschrift für Flugtechnik und Motorluftschiffahrt 16(10):206–208

Thwaites B (1960) Incompressible aerodynamics. Clarendon Press, Oxford. ISBN 978-0486654652

van Holten T (1981) Concentrator systems for wind energy, with emphasis on tip-vanes. Wind Eng 5(1):29–45

van Kuik GAM (2017) Joukowsky actuator disc momentum theory. Wind Energy Sci 2:307–316. ISSN 2366-7621. https://doi.org/10.5194/wes-20l6-55

van Kuik GAM (2018a) Comparison of actuator disc flows representing wind turbines and propellers. J Phys Conf Ser 1037(Torque2018):1–10

van Kuik GAM (2018b) The fluid dynamic basis for actuator disc and rotor theories, open acces edition. IOS Press, Amsterdam. ISBN 978-1-61499-865-2. https://doi.org/10.3233/978-1-61499-866-2-i

van Kuik GAM, Lignarolo LEM (2016) Potential flow solutions for energy extracting actuator disc flow. Wind Energy 19:1391–1406. https://doi.org/10.1002/we1902

van Kuik GAM, Yu W, Sarmast S, Ivanell S (2015a) Comparison of actuator disc and Joukowsky rotor flows, to explore the need for a tip correction. J Phys Conf Ser 625:012013. https://doi.org/10.1088/1742-6596/625/1/012013

van Kuik GAM, Sørensen JN, Okulov VL (2015b) Rotor theories by Professor Joukowsky: momentum theories. Progress Aerospace Sci 73:1–18. ISSN 03760421. https://doi.org/10.1016/j.paerosci.2014.10.001

von Kármán T, Burgers TM (1935) Motion of a perfect fluid produced by external forces. In: Aerodynamic theory, vol *Π* Division *E* Chapt. IIIA. Springer, Berlin

Wilmshurst S, Metherell AJF, Wilson DMA, Milborrow DJ, Ross JN (1984) Wind turbine rotor performance in the high thrust region. In: Sixth BWEA conference, 1984

Wood DH (2007) Including swirl in the actuator disk analysis of wind turbines. Wind Eng 31(5):317–323.

Wood DH (2015) Maximum wind turbine performance at low tip speed ratio. J Renew Sustain Energy 7:053126. https://doi.org/10.1063/1.4934895

Xiros MI, Xiros NI (2007) Remarks on wind turbine power absorption increase by including the axial force due to the radial pressure gradient in the general momentum theory. Wind Energy 10(1):99–102. ISSN 10954244. https://doi.org/10.1002/we203